AMEGHINIANA
A GONDWANAN PALEONTOLOGICAL JOURNAL

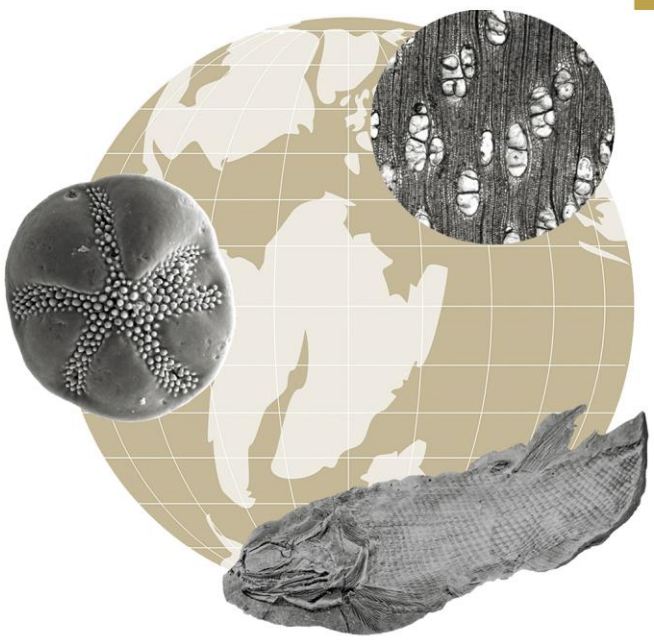

Submitted: 30 October 2025 - **Accepted**: 8 September 2026 - **Posted online**: 8 September 2026

To link and cite this article:

doi: 10.5710/AMGH.08.09.2026.3677

Advances on the paleobiology of Upper Triassic Argentinean Proterochampsidae (Archosauriformes): growth dynamics, intraspecific variation, and palaeoecology

Denis A. Ponce[1*], Laureano Carivali[2], Jordi A. Garcia Marsà[3] and Julia B. Desojo[4]

[1]Instituto de Investigación en Paleobiología y Geología (IIPG), CONICET-Universidad Nacional de Río Negro, Av. J.A. Roca 1242, 8332, General Roca, Río Negro, Argentina; Museo 'Carlos Ameghino', Belgrano 1700, Paraje Pichi Ruca (predio Marabunta), 8324, Cipolletti, Río Negro, Argentina. denispunrn@yahoo.com.ar

[2]Facultad de Ciencias Naturales y Museo, Universidad Nacional de La Plata, Av. 122 & 60, B1900, La Plata, Buenos Aires, Argentina.

[3]CONICET-Laboratorio de Anatomía Comparada y Evolución de los Vertebrados, Museo Argentino de Ciencias Naturales "Bernardino Rivadavia", Ángel Gallardo 470, C1405DJR, Ciudad Autónoma de Buenos Aires, Argentina.

[4]CONICET-División Paleontología Vertebrados, Facultad de Ciencias Naturales y Museo, Universidad Nacional de La Plata, Paseo del Bosque $^{S}/_{N^{\circ}}$, B1900FWA, La Plata, Buenos Aires, Argentina.

35 pages (text + references); 8 figures; 2 tables.

Running header: PONCE ET AL.: Bone histology of Argentinean proterochampsids.

Short description: Proterochampsid histology indicates diverse growth modes and ecological specializations preceding early archosaur evolution.

Corresponding author: Denis Alejandro Ponce, Instituto de Investigación en Paleobiología y Geología (IIPG), CONICET-Universidad Nacional de Río Negro, Av. J.A. Roca 1242, 8332, General Roca, Río Negro, Argentina; Museo 'Carlos Ameghino', Belgrano 1700, Paraje Pichi Ruca (predio Marabunta), 8324, Cipolletti, Río Negro, Argentina. Email address: denispunrn@yahoo.com.ar

Abstract. Proterochampsids were small to medium size carnivorous quadrupedal archosauriforms from the Middle–Upper Triassic of America. In Argentina, they are distributed in the Ischigualasto-Villa Unión Basin. Here, we describe the bone histology of Argentinean proterochampsids *Proterochampsa barrionuevoi* PVSJ 606 (humerus), *Tropidosuchus romeri* PVL 4602 (femur), *Gualosuchus reigi* PVL 4576 (humerus, femur and tibia) and *Chanaresuchus bonapartei* PVL 4575 (humerus and tibia) and PVL 6244 (humerus, femur, dorsal rib) to infer growth dynamics (using qualitative and quantitative approaches), inter and intraspecific variation and lifestyle (using statistical models). *Proterochampsa* and *Tropidosuchus* reached a moderate–fast growth, based in woven-fibred bone tissue and radial-longitudinal vascularisation, although *Proterochampsa* exhibits an external fundamental system, indicating growth cessation. *Gualosuchus* displays fibrolamellar complex highly vascularised during early stages of its ontogeny, indicative of rapid growth. Individuals of *Chanaresuchus* show disparate growth strategies, characterized by parallel-fibred bone tissue alone or in association with patches of woven-fibred bone, together with moderate to high levels of vascularization. Therefore, proterochampsids present a notable diversification in their growth strategies, which is reflected between species and within the individuals (specially marked in *Chanaresuchus*). Quantitative analyses indicate irregular growth rates, similar to those of extant crocodiles. Analyses of the lifestyle suggest a differentiation in the divergence of Proterochampsidae subfamilies, with Proterochampsinae (*Proterochampsa*) as amphibious/aquatic and Rhadinosuchinae (*Chanaresuchus, Gualosuchus* and *Tropidosuchus*) as terrestrial. These findings provide new insights into the palaeobiology and ecological diversification of Proterochampsidae, shedding light on the evolutionary pathways that preceded the emergence of crown-group Archosauria.

Keywords. Argentina, bone histology, *Chanaresuchus*, growth rate, lifestyle, *Proterochampsa*, Triassic, *Tropidosuchus*.

Resumen. Avances en la paleobiología de los Proterochampsidae (Archosauriformes) del Triásico Superior argentino: dinámica de crecimiento, variación intraespecífica y paleoecología. Los proterocámpsidos fueron arcosauriformes cuadrúpedos carnívoros de tamaño pequeño–mediano del Triásico Medio–Superior de América. En Argentina, se distribuyen en la Cuenca Ischigualasto-Villa Unión. Aquí describimos la histología ósea de los proterocámpsidos *Proterochampsa barrionuevoi* PVSJ 606 (húmero), *Tropidosuchus romeri* PVL 4602 (fémur), *Gualosuchus reigi* PVL 4576 (húmero, fémur, tibia) y *Chanaresuchus bonapartei* PVL 4575 (húmero, tibia) y PVL 6244 (húmero, fémur, costilla dorsal), para inferir dinámicas de crecimiento (mediante enfoques cualitativos y cuantitativos), variación intra e interespecífica y estilos de vida (empleando modelos estadísticos). *Proterochampsa* y *Tropidosuchus* alcanzaron un crecimiento moderado–rápido, basado en su tejido óseo fibrolamelar y vascularización radial y longitudinal y *Proterochampsa* presenta un sistema fundamental externo, señal de crecimiento detenido. *Gualosuchus* desarrolló tejido fibrolamelar altamente vascularizado, indicativo de crecimiento rápido en las etapas tempranas de su desarrollo. Los individuos de *Chanaresuchus* exhiben un crecimiento dispar, con hueso entrejido unicamente o asociado a parches de hueso pseudolamelar y vascularización moderada a abundante. Así, los proterocámpsidos muestran una marcada diversificación en sus estrategias de crecimiento entre especies e individuos (especialmente en *Chanaresuchus*). Análisis cuantitativos indican tasas de crecimiento irregulares, similares a las de cocodrilos actuales. Análisis del modo de vida sugieren una divergencia ecológica entre subfamilias, con Proterochampsinae (*Proterochampsa*) como formas anfibias y acúaticas y Rhadinosuchinae

(*Chanaresuchus*, *Gualosuchus*, *Tropidosuchus*) como terrestres. Estos resultados aportan nueva información sobre la paleobiología y diversificación ecológica de Proterochampsidae y su papel en las trayectorias evolutivas previas al origen de Archosauria.

Palabras clave. Argentina, *Chanaresuchus*, estilo de vida, histología ósea, *Proterochampsa*, tasa de crecimiento, Triásico, *Tropidosuchus*.

Introduction

Proterochampsidae is a family of non-archosaurian Archosauriformes from the Middle–Upper Triassic (middle Ladinian–late Norian) deposits from America (Trotteyn et al., 2013). They were small to medium size quadrupedal osteoderm-bearing forms, superficially resembling crocodiles (Trotteyn et al., 2013). Its phylogenetic position has been difficult to assess in the past, but recent studies recovered Proterochampsidae as the sister taxon of Doswelliidae and both are included within Proterochampsia, the sister taxon of Archosauria (Ezcurra et al., 2021; Simão-Oliveira et al., 2022; Müller, 2025).

The proterochampsids come mostly from two Triassic basins from Argentina and Brazil, the Ischigualasto-Villa Unión Basin and the Paraná Basin, respectively. The Ischigualasto-Villa Unión Basin includes five species from two geological units. First, the early–middle Carnian Chañares Formation records *Chanaresuchus bonapartei* Romer, 1971; *Gualosuchus reigi* Romer, 1971 and *Tropidosuchus romeri* Arcucci, 1990, and the late Carnian–early Norian Ischigualasto Formation contains *Proterochampsa barrionuevoi* Reig, 1959 and *Pseudochampsa ischigualastensis* Trotteyn and Ezcurra, 2014. In the Paraná Basin, six formally named proterochampsids that come from three different horizons, here classified as ‘sequences’, are identified. In the late Ladinian–early Carnian Pinheiros-Chiniquá Sequence are recovered *Pinheirochampsa rodriguesi* Paes-Neto et al., 2024 and *Retymaijychampsa beckerorum*

Müller, 2025. The early to middle Carnian Santa Cruz Sequence registers *Kuruxuchampsa dornellesi* Paes-Neto et al., 2024. Otherwise, the middle Carnian–late Norian Candelária Sequence records *Cerritosaurus binsfeldi* Price, 1946; *Rhadinosuchus gracilis* von Huene, 1938 and *Proterochampsa nodosa* Barberena, 1982. Finally, *Sphodrosaurus pennsylvanicus* Colbert, 1960 remains as a species with ambiguous phylogenetic relations. Different analyses recovered it as a non-Proterochampsidae Proterochampsia (Ezcurra and Sues, 2021), whereas in others is considered a stem Proterochampsidae (Paes-Neto et al., 2024).

Because of their close phylogenetic relationships with Archosauria (Ezcurra et al., 2021; Simão-Oliveira, et al., 2022; Müller, 2025), the study of proterochampsids allows to understand the evolutive history of the early archosauriformes lineages toward archosaurs before the Triassic–Jurassic extinction. Investigate the paleobiology and growth patterns of Proterochampsidae to understand what features may have evolved in this group and also prevailed in Archosauria.

Most of the palaeobiological studies performed in proterochampsids focused in the osteohistological topics (Ponce et al., 2017, 2021; Arcucci et al., 2019; Garcia Marsà et al., 2020, 2023; Curry Rogers et al., 2024) and a few, researched on their biomechanics (Simão-Oliveira et al., 2024). Recently, Cotuli-Cereda et al. (2026) suggested an intermediate transitive state between the primitive mesotarsal type of basal archosauriforms and the advanced meso-tarsal tarsus of ornithodirans for *Chanaresuchus bonapartei*. The osteohistological aspects of several proterochampsid exhibit a striking diversity regarding growth dynamics, varying in a range from slow to intermediate rates during their rather complete ontogeny, and a few are reported even faster (Arcucci et al., 2019; Garcia Marsà et al., 2020, 2023; Ponce et al., 2021; Curry Rogers et al., 2024). Nevertheless, the microstructure of some species remain unknown

and quantitative histological studies are scarce. Furthermore, the lifestyle of proterochampsids is a broadly debated issue because of the occurrence of ambiguous anatomical features, such as relatively sturdy and long limbs and presumably semi-erect or sprawling posture (Simão-Oliveira et al., 2024; Trotteyn and Paulina-Carabajal, 2016; Ezcurra et al., 2021). However, recent studies based in statistical methods and microanatomical data inferred a terrestrial habit for some rhadinosuchines, such as *C. bonapartei*, and *Tropidosuchus romeri* (Ponce et al., 2021; Garcia Marsà et al., 2023).

This study aims to examine the bone histology of appendicular and axial bones of Argentinean proterochampsids unreported to date, such as *Gualosuchus reigi*, as novel elements of other species previously studied such as *Chanaresuchus bonapartei*, *Proterochampsa barrionuevoi* and *Tropidosuchus romeri* as well (Fig. 1). As informed in prior research (Arcucci et al., 2019; Garcia Marsà et al., 2020, 2023; Ponce et al., 2021; Curry Rogers et al., 2024), bone histology is expected to record a great intra and interspecific variation in its growth dynamics. Additionally, we expect to infer the lifestyle of *G. reigi, P. barrionuevoi* and *Pseudochampsa ischigualastensis* employing statistical models. For this goal, we propose that rhadinosuchines (i.e., *G. reigi, P. ischigualastensis*) possessed a terrestrial habit, in contrast with an aquatic or amphibious lifestyle estimated for proterochampsines (i.e., *P. barrionuevoi*). Finally, we quantitatively compare growth patterns from: the cumulative growth and the growth rates, at daily and annual scale. Given their morphological and ecological resemblance to crocodiles, similar values for these variables are expected.

Institutional abbreviations: CRILAR-Pv, Centro Regional de Investigaciones Científicas y Técnicas de La Rioja, La Rioja, Argentina; PVL, Instituto Miguel Lillo, S.M. de Tucumán, Tucumán, Argentina; PVSJ, División Paleontología de Vertebrados, Museo de Ciencias Naturales, Universidad Nacional de San Juan, San Juan City, San

Juan, Argentina; PULR-V, Museo de Ciencias Naturales de la Universidad Nacional de La Rioja, La Rioja City, La Rioja, Argentina.

Material and methods

Materials

For the current study, several thin sections of appendicular and axial bones of Argentinean proterochampsids are histologically examined. These include *Proterochampsa barrionuevoi* PVSJ 606 (holotype), *Tropidosuchus romeri* PVL 4602, *Gualosuchus reigi* PVL 4576 and *Chanaresuchus bonapartei* PVL 6244 (Fig. 1). The specific sampled elements and their provenance are shown in Table 1. All specimens were partially or totally described in prior research, including reviews of their original anatomical description and/or used as comparative material in major studies (Trotteyn et al., 2013; Ezcurra et al., 2010; Trotteyn and Ezcurra, 2014; Ezcurra, 2016).

Methods

To prepare the slides, we followed standardized protocols for petrographic thin sections (Cerda et al., 2020) and these are performed in the Laboratorio de Paleohistología of the Museo Paleontológico Carlos Ameghino (Cipolletti, Río Negro, Argentina). When possible, the planes of section were chosen to prioritize regions with an extensive cortical growth record (Sander et al., 2004) and, in this sense, the appendicular bones were sectioned at the diaphyseal region. The slides were analysed with a petrographic microscope (Nikon E200 Pol, Leica DM750P) under plane and cross-polarised light, using a lambda filter for the latter (λ). For the terminology of growth marks, vascularisation and bone matrix, we follow the nomenclature proposed by Buffrénil and Quilhac (2021).

183 To estimate the lifestyle of the sampled specimens, several parameters
184 calculated by the R version of Bone ProfileR (Girondot and Laurin, 2003; Gônet et al.,
185 2022) are introduced into predictive statistical models based on linear discriminant
186 analysis. With this package, it is possible to obtain the 'observed compactness' (OC),
187 the ratio (values between 0 and 1) of the cross-sectional area that includes bone tissue
188 and spaces or cavities from binarized images (i.e., black colour: bone, white colour:
189 spaces and cavities) of complete transverse sections.
190 Likewise, Bone ProfileR generates a 'compactness profile' which contains
191 several parameters. This profile consists of a sigmoid curve, which represents the
192 distribution of bone compactness from the medullary centre to the outermost limit of the
193 cortex. The results of this analysis include, among other parameters: the slope at the
194 inflection of the curve (S), the location of the inflection point of the curve on the x-axis
195 (P), the lowest (Min) and highest (Max) compactness values and their asymptote, the
196 observed compactness (OC) and the modelled or predicted compactness (MC). Bone
197 Profiler also provides an angular or radial analysis and its corresponding parameter
198 values: radial slope (RS), radial inflection point (RP) and minimum (R_{Min}) and
199 maximum (R_{Max}) radial values of compactness.
200 The models to infer the lifestyles are based on linear discriminant analysis and
201 yield two and three possible lifestyles, and they are therefore referred to as (1) binary
202 statistical model (BSM) for the humeri (Canoville and Laurin, 2010) and (2) ternary
203 statistical model (TSM) for the femora (Quémeneur et al., 2013), respectively. The
204 resources to test the models (i.e., automatic Excel spreadsheet with linear discriminant
205 variables) are available in the supplementary material of these studies. Similar methods
206 have been proposed to infer lifestyle in extinct and living taxa using different
207 appendicular bones (Laurin et al., 2004; Germain and Laurin, 2005; Kriloff et al., 2008;

Canoville and Laurin, 2009; Canoville and Laurin, 2010; Laurin and Buffrénil, 2015). The accuracy of these models varies depending on the skeletal elements considered, but these exhibit a strong confidence in general, since their predictions are based in extant taxa observations. In specific, the accuracy is 85% for the femur of lissamphibians (Laurin et al., 2004), 70.6% for the radius of amniotes (Germain and Laurin, 2005), 63% for the tibia of amniotes (Kriloff et al., 2008), 89.2% for the humerus of lissamphibians (Canoville and Laurin, 2009), 98.5% for the humerus of amniotes (Canoville and Laurin, 2010) and 88% for the femur of amniotes (Quémeneur et al., 2013). The models combine microanatomical data calculated by Bone ProfileR analysis (i.e., values for the parameters S, P, CO, CM, R_{min}, and R_{max}) and morphological data, the snout–vent length (SVL). To estimate the SVL in extinct vertebrate we used an equivalent measurement based on the presacral length, the extension from the tip of the snout to the last dorsal vertebra. Once these data are entered into the models, the prediction can assume one of two possible lifestyle states for the BSM: 0 (aquatic) and 1 (amphibian/terrestrial) (Canoville and Laurin, 2010), and three for TSM: 0 (aquatic), 1 (amphibian), and 2 (terrestrial) (Quémeneur et al., 2013). States are defined by the relative amount of time spent in water: >90% for an aquatic taxon, between 20% and 90% for an amphibian taxon, and <20% for a terrestrial taxon (Laurin et al., 2004).

To estimate growth rates using quantitative approaches, we employed basic methods based on skeletochronology. We used femoral bones from several proterochampsid specimens, including those reported here and others informed in previous studies (Garcia Marsà et al., 2020, 2023; Ponce et al., 2021; Curry Rogers et al., 2024). Cyclical growth marks (CGM) reflect periodic variations in the rate of osteogenesis (e.g., Francillon-Vieillot et al., 1990; Castanet et al., 1993; Castanet et al.,

2000; Chinsamy-Turan, 2005; Chinsamy 2023) of the individuals, and can therefore be used as a measure to approximate the dimensional growth.

Otherwise, given the absence of presumed juvenile individuals and a relatively complete ontogenetic series for proterochampsid species, simple variables such as the perimeter and area for cumulative growth and annual and daily growth rates are calculated. This method is partially based in previous studies (Woodward et al., 2014; Fernández Dumont et al., 2021; Audije-Gil et al., 2023; Pereyra et al., 2025) and allow us to provide preliminary inferences. Prior to growth rate analysis, severely deformed sections are retro-deformed to restore to their original ellipsoid-like shape to achieve a suitable dimensional handle using Adobe Photoshop. Subsequently, the contours of the CGM, as well as the contours of the medullary cavity (MC) and the subperiosteal surface (SPS), are traced also with Photoshop (Fig. S1). However, only those CGM that are continuous throughout the cortex are considered for the analyses. The CGM that are not fully traceable are dismissed, although they are mentioned for each section. To calculate the cumulative perimeter and area, the extension of the contour and the surface enclose by the MC, the successive CGM and the SPS are calculated for each section using ImageJ (Schneider et al., 2012) software. To calculate the annual growth rate contained between the growth marks, the perimeter and the area of each successive CGM was subtracted from the immediately prior CGM (i.e., $CGM_{(n+1)}$-CGM_n) (Fig. S2). Finally, to calculate the daily growth rate, these results are divided into the number of days of a calendar year during Late Triassic (Carnian). Wu et al. (2024) calculated this value to be 382 days, based on an estimated day length of 23 hours 220 Ma. To visualize the resulting data, we plotted ‘lines with markers’ graphs using Microsoft Office Excel.

Results

Histological descriptions

Proterochampsa barrionuevoi PVSJ 606: a transverse section of the humerus extracted from the diaphysis (Fig. 2A) was examined. The element retains its original circular-like shape in general and shows a poor state of preservation. Some portions of the cortex are eroded and are crossed by several fractures (Fig. 2A). Hence, the matrix is observable only in specific areas. The section exhibits a relatively small free marrow cavity, followed by a thicker cortex (Fig. 2A, B). In the perimedullary cortex, some secondary osteons and resorption spaces are surrounded by lamellar bone (Fig. 2B, C), which gradually disappear towards the middle cortex (Fig. 2B, C). The remaining cortex is mainly composed by woven-fibred bone marked by a random organisation and rounded shape of the osteocyte lacunae (when these are visible enough) and its isotropic condition under cross-polarised light (Fig. 2D–F). Vascularisation is rather moderate, with radial canals being predominant and longitudinal and circumferential canals (reaching a reticular pattern in some areas) and some primary osteons observed to a lesser extent (Fig. 2B–F). No growth marks are recorded within the cortex; however, an avascular external fundamental system (EFS) is present (Fig. 2G).

Tropidosuchus romeri PVL 4602: the sample is a transverse section of the femoral shaft (Fig. 3A, B). The section is fragmented and fractured into several parts and it is slightly compressed in the lateral and medial regions (Fig. 3A, B), hence, the bone matrix is moderately visible (Fig. 3A, B). The medullary cavity is free (Fig. 3A, B) and the cortical tissue occupies approximately half of the total radius of the section. The cortex is formed by woven-fibred bone; however, due to taphonomic artifacts, it appears moderately anisotropic under crossed-polarised light in some areas (Fig. 3C, D). When observable, the osteocyte lacunae are dispersed and have a subrounded shape. The inner

and middle cortex is highly vascularised, comprising longitudinal, circumferential, and radial canals, acquiring a reticular pattern in some areas. Towards the subperiosteal cortex, vascularisation is reduced (Fig. 3C, D). No growth marks or signs of bone remodelling are recorded.

Gualosuchus reigi PVL 4576: the samples include transverse sections of the shafts of the humerus (Fig. 4A), femur (Fig. 4B) and tibia (Fig. 4C). All three elements are well preserved in general, retaining their original shape, showing no fractures, and the matrix is clearly visible. Only the humerus had lost a small portion of cortex from the anterior margin, but all three bones share the same histological features (Fig. 4A). The medullary cavity and the cortical tissue occupy approximately one-third of the total radius of the section (Fig. 4A–C). They are composed of the fibrolamellar complex homogeneously distributed throughout the cortex (Fig. 4D–F). Osteocyte lacunae are plentiful, randomly organised and possess a globular-like shape (Fig. 4D–F). Abundant primary osteons and vascular canals are also present, mostly oriented longitudinally, although some radial and circumferential canals are observed as well (Fig. 4D–F). No growth marks or signs of bone remodelling are recorded.

Chanaresuchus bonapartei PVL 4575: the samples consist of transverse sections of the humerus (Fig. 5A) and the tibia (Fig. 5B), sectioned from the diaphysis. Both elements are affected by multiple fractures and are strongly compressed lateromedially, with the medullary cavity invaded by fragments of the cortex (Fig. 5A, B). The compacta is composed of parallel-fibred bone in the humerus (Fig. 5C). This feature is evident because of the elongated shape of the osteocyte lacunae, their orderly distribution and a marked anisotropy of the matrix under cross-polarised light (Fig. 5C). However, in certain areas, the anisotropy becomes less pronounced, the osteocyte lacunae acquire a more ellipsoid-like shape and display a more dispersed and random organisation (Fig.

5D), acquiring a woven-fibred bone appearance. The tibia is entirely composed of parallel-fibred bone (Fig. 5E). Both elements are highly and uniformly vascularised with numerous longitudinal, circumferential, and oblique canals arranged in a reticular pattern in the humerus (Fig. 5C, D) and in a rather laminar to subplexiform pattern in the tibia (Fig. 5E). Three lines of arrested growth (LAGs) are recognised in the humerus, the first two located in the perimedullary region, and the last in the middle cortex (Fig. C). No cyclical growth marks (CGM) are observed in the tibia, and an EFS is absent in both elements.

Chanaresuchus bonapartei PVL 6244: samples include transverse sections of the humerus (Fig. 5F) and femur (Fig. 5G), both extracted from the shaft. A dorsal rib was also included (Fig. 5H), but no photographs were obtained prior to sectioning. Both appendicular elements are cracked and severely deformed since lateral and medial portions of the bones are strongly compressed toward the marrow cavity (Fig. 5F, G). Consequently, the latter is obliterated by fragments of the cortex (Fig. 5F, G). Despite these taphonomic conditions, the bone matrix is clearly visible. This is mostly composed of concentric layers of highly anisotropic (i.e., strong birefringence) parallel-fibred bone, alongside minor layers of slightly anisotropic (i.e., weak birefringence) parallel-fibred bone (Fig. 5I, J). This arrangement gives to the cortex a stratified appearance under crossed-polarised light (Fig. 5I, J). The separation between the layers is marked by the differences in the vascularisation and the CGM (read below). Moreover, the osteocyte lacunae possess an elongated shape and reduce their density toward the subperiosteal margin.

The degree of vascularisation in both appendicular elements is variable. Thus, in the layers surrounding the cortex, vascularisation ranges from poor to moderate, dominated by some circumferential and longitudinal canals (Fig. 5I, J). In the mid-

portion of the cortex, vascularisation is more profuse and it is formed by circumferential and longitudinal canals mainly, accompanied by some radial canals (Fig. 5I, J). Near subperiosteal region, the vascularisation becomes scarce again (Fig. 5I, J). However, the femur exhibits an additional thin layer with abundant circumferential canals deposited on the outer cortex (Fig. 5J). Likewise, while the arrangement of the vascular canals generates laminar pattern in some portions of the femur (Fig. 5J), none particular orientation is recognised in the humerus (Fig. 5I). Three lines of arrested growth (LAGs) are recorded in the humerus, the first two located in the perimedullary region and the last placed in the subperiosteal cortex (Fig. 5I). Meanwhile, up to six growth marks (LAGs and annuli) are registered in the femur, the first located in the perimedullary region and the rest of them are placed in the subperiosteal region (Fig. 5J).

The dorsal rib is also deformed (Fig. 5H), since it was presumably affected in two adjacent points in the cortex (Fig. 5H). The bone matrix is poorly preserved and it is visible in a few specific areas. The section features two distinct regions: a medullary cavity of cancellous bone and a thick cortex of compact tissue (Fig. 5H, K). However, the former is severely affected by fossil-diagenetic processes, and most of the cancellous bone has been eroded, except for a few isolated trabeculae (Fig. 5K). In the perimedullary region of the compact cortex, woven-fibred bone of primary origin with simple canals are observed, accompanied by some isolated secondary osteons (Fig. 5K). The osteocyte lacunae of the woven-fibred bone possess a rounded-like shape and are randomly arranged (Fig. 5K). Towards the middle and external portion of the cortex, there is recorded lamellar bone, slightly vascularised with some simple canals (Fig. 5K). Covering this layer, up to eight tightly grouped LAGs are recorded, indicative of an EFS (Fig. 5K).

Lifestyle analyses

To evaluate the habit, besides several of the samples above mentioned, we also evaluated femoral sections of *Pseudochampsa ischigualastensis* PVSJ 567 and *Proterochampsa barrionuevoi* PVSJ 606, histologically described in previous studies (Curry Rogers et al., 2024). The sections of *Chanaresuchus bonapartei* (PVL 4575 and PVL 6244) are dismissed from this method because (1) analysis of the femur (PVL 4575) was already performed, resulting in terrestrial lifestyle (Ponce et al., 2021) and (2) unlike CGMs that are simply contours of the cortex, vascularisation is far sensitive to a possible retrodeformation. Rearrangement of cortex might severely affect the original distribution of canals and lead to an over or sub estimation of the compactness. For this reason, Bone ProfileR reaches robust analyses when sections are rather well preserved and deformation is minimal (Girondot and Laurin, 2003; Gônet et al., 2022). Hence, we implemented this method for a total of six well preserved elements: humerus and femur of *Gualosuchus reigi* PVL 4576 and *P. barrionuevoi* PVSJ 606, and femur of *Gualosuchus reigi* PVL 4575 and *Tropidosuchus romeri* PVL 4602 (Table S1). Likewise, the snout–vent length was obtained for the first hand, measuring 352 mm for *G. reigi* PVL 4576, 464 mm for *P. barrionuevoi* PVSJ 606, 357 mm for *P. ischigualastensis* PVSJ 567 and 286 mm for *T. romeri* PVL 4602.

The specific values for the parameters S, P, CO, R_{min}, and R_{max} extracted from the results of Bone ProfileR are detailed in the Table S1. Furthermore, Figure 6 displays the binarized sections and the compactness profiles of the selected elements. The binary statistical model (BSM), based on the humerus (Canoville and Laurin, 2010), yielded 'state 1', indicating an amphibious/terrestrial habitat for both *P. barrionuevoi* PVSJ 606 and *G. reigi* PVL 4576. The ternary statistical model (TSM), based on the femur (Quémeneur et al., 2013), resulted in a terrestrial lifestyle ('state 2') for *T. romeri* PVL

4602, *G. reigi* PVL 4576 and *P. ischigualastensis* PVSJ 567, but thrown an aquatic habitat ('state 0') for *P. barrionuevoi* PVSJ 606.

Quantitative analyses

We obtained numerical growth data from the femoral sections of *Chanaresuchus bonapartei* PVL 6244 histologically described here, and other five specimens, previously reported in the literature (Garcia Marsà et al., 2020, 2023; Ponce et al., 2021; Curry Rogers et al., 2024): *C. bonapartei* PULR-V 125 and, *Pseudochampsa ischigualastensis* PVSJ 567, *Rhadinosuchinae* indet. CRILAR-Pv 488, and *Tropidosuchus romeri* PVL 4604 and PVL 4606 (Table S2, Fig. S1). Several of these lack fully traceable CGM. Additionally, four other specimens, *C. bonapartei* (PVL 4575), *Gualosuchus reigi* (PVL 4576), *Proterochampsa barrionuevoi* (PVSJ 606) and *T. romeri* (PVL 4602), were initially considered for this analysis, but were excluded because CGM are absent or they are not fully traceable (Table S2). Furthermore, the Figure 7 shows the graphs of the cumulative perimeter and area growth, annual perimeter and area growth rates and daily perimeter and area growth rates.

Discussion

Disparate growth patterns

Since we are dealing with a moderate in number and variable bone elements and our intention is to compare those of previous reports, we are forced to homogenise the analysed elements to achieve constant inferences. Hence, given that femur is the most repeated bone across the sample and in previous studies, we select this element as proxy for its evaluation. Next, we classify the growth rate based in qualitative histological features employing parameters related with intrinsic fibres organisation of the osseous matrix and vascular canals organisation and density.

In general, the specimens here analysed and those from the literature show CGM, therefore a cyclical growth is inferred for them. An overall fast growth rate is estimated for a few specimens, such as Proterochampsidae indet. CRILAR-Pv 118, 603 and 603 (Arcucci et al., 2019), *Tropidosuchus romeri* PVL 4604 (Garcia Marsà et al., 2020) and *Gualosuchus reigi* PVL 4576, which exhibit a fibrolamelar complex composition and abundant vascularisation. Other relatively rapid growth includes that of stratified nature of the cortex. This is named zonal bone, where zones of highly vascularised fibrolamelar complex or woven-fibred bone and annuli of poorly vascularised parallel-fibred bone are distributed in thick and thin layers respectively. This implies a marked condition of cyclical growth. Specimens such as *Chanaresuchus bonapartei* PULR-V 125 (Garcia Marsà et al. 2020) and PVL 6244 and Rhadinosuchinae CRILAR-Pv 488 (Ponce et al., 2021) show this configuration. The two latter, record an accelerated growth stage late in ontogeny. Furthermore, a minor, but rapid growth rate as well, based in the presence of woven-fibred bone and modest radial and rather reticular vascularisation is inferred for *Proterochampsa barrionuevoi* PVSJ 606 (Curry Rogers et al., 2024) and *T. romeri* PVL 4602. A rather moderate to slightly-rapid growth rate, reflected by a cortex dominated by parallel fibred-bone with patches of woven-fibred bone and a strong vascularisation, is registered in *C. bonapartei* PVL 4575 (Ponce et al., 2021). A variation of this kind of growth is reported in *C. bonapartei* PULR-V 116 and *T. romeri* PVL 4606 specimen (Garcia Marsà et al., 2023), where patches of woven-fibred are absent, evidence of a lower growth rate. Finally, the slowest growth rate, which feature parallel-fibred bone matrix and moderate vascularisation, is indicated for *Pseudochampsa ischigualastensis* PVSJ 605 (Curry Rogers et al., 2024).

As seen, a marked disparity is observed regarding osteohistological traits for the femora in Argentinian Proterochampsidae. Therefore, a common growth strategy for the group seems uncertain. In addition, since a single individual of *Gualosuchus romeri*, *Pseudochampsa ischigualastensis* and *Proterochampsa barrionuevoi* was examined, future studies should increase sampling to determine the nature of such degree of variation. Nevertheless, some specific inferences are noted for *G. romeri* and *P. barrionuevoi*. In particular, *G. romeri* reports the most accelerated growth for Proterochampsidae without bone remodelling, likely indicative of a juvenile stage for this individual. Likewise, the unique histological features registered in femur (Curry Rogers et al., 2024) and humerus of *P. barrionuevoi*, are possible related with its lifestyle (see below).

Regarding the observed diversity in femora, *Chanaresuchus bonapartei* and *Tropidosuchus romeri* specimens display different bone tissue arrangements. As state in Table 2, these include fast (*T. romeri* PVL 4604), fast with a marked cyclicity (*C. bonapartei* PULR-V 125 and PVL 6244), moderate to slightly-rapid (*C. bonapartei* PULR-V 116 and PVL 4575 and *T. romeri* PVL 4606) and moderate growth (*T. romeri* PVL 4602) (Garcia Marsà et al., 2020, 2023; Ponce et al., 2021). In consequence, *T. romeri* and *C. bonapartei* show some degree of variation between the individuals, being more pronounced in the latter.

As typical for archosaurs, rapid growth, marked by the presence of highly vascularised fibrolamellar complex or woven-fibred bone, is expressed in early stages of ontogeny (Padian and Stein, 2013; Chinsamy, 2023). Later in ontogeny, the growth rate decreases, generating poor vascularised or avascular parallel-fibred or lamellar bone (Padian and Stein, 2013; Chinamy, 2023). This pattern is diffuse in the individuals of *T. romeri* and it is lacking in the specimens of *C. bonapartei* and a correlation between

457 bone tissue traits and dimensional growth is rather absent (Table 2). For example,
458 relatively small specimens are formed almost entirely of parallel-fibered bone, a tissue
459 type generally associated with moderate growth during late stages of ontogeny (Table 2)
460 (Garcia Marsà et al., 2023). The individual *C. bonapartei* PULR-V 116 fits well within
461 this pattern: with a femur length of 71 mm, represents 47% of the largest femur length
462 reported for the species (i.e., 151 mm, in PVL 6244). Strikingly, however, larger
463 specimens, which are likely older, exhibit the opposite pattern. Indeed, *C. bonapartei*
464 PVL 6244 and *T. romeri* PVL 4602 both show fibrolamellar complex (Garcia Marsà et
465 al., 2020). The femur of *T. romeri* PVL 4602 measures 55 mm of length, which
466 represents 88% of the largest femur length reported for the species (68 mm, in PVL
467 4606) (Mamani, 2026). Given that fibrolamellar bone typically reflects fast growth in
468 early stages, its presence in such large specimens is unexpected.
469 Ruling out an ontogenetic explanation, these variations are plausibly attributable
470 to some degree of developmentally flexibility growth in the growth, which may be
471 related to several, but not mutually exclusive, causes (e.g., body size, habitat, sexual
472 dimorphism, environmental pressure). For example, it was inferred recently that captive
473 and wild specimens of extant *Caiman yacare* exhibit a diversity in its growth modes
474 linked to an environmental pressure component (i.e., resources availability?) and a
475 highly physiological susceptibility (Pereyra et al., 2025). In this sense, it possible that
476 *Tropidosuchus romeri* and *Chanaresuchus bonapartei* presented the same strategy.
477 In this sense, here we use the more descriptive term *developmentally flexible*
478 *growth* to refer to variation in growth trajectories inferred from osteohistological data.
479 Comparable patterns have frequently been interpreted as manifestations of
480 developmental plasticity in the vertebrate osteohistological literature (e.g., Starck and
481 Chinsamy, 2002; Sander and Klein, 2005; Sanchez et al., 2010; McHugh, 2015;

Chapelle et al., 2021; Cerda et al., 2022; Marsà et al., 2023). We follow a more descriptive terminology because the concept of developmental plasticity is now widely used in evolutionary developmental biology (evo-devo), ecological developmental biology (eco-devo), and related disciplines to describe environmentally mediated developmental responses whose underlying developmental mechanisms can be investigated experimentally in extant taxa (e.g., West-Eberhard, 2003; Beldade et al., 2011). Nevertheless, hypotheses suggesting developmental plasticity in extinct taxa may still be legitimately evaluated through the consilience of multiple independent lines of evidence, such as osteohistology, comparative anatomy, phylogenetic inference and paleoenvironmental reconstructions, rather than through any single proxy considered in isolation (e.g., Wilson, 1998; Cleland, 2002).The wide range of growth strategies estimated in proterochampsids indicates that highly variable physiological adaptations were relatively common in Upper Triassic tetrapods. For instance, the gracilisuchid *Gracilisuchus stipanicicorum* and the erpetosuchid *Tarjadia ruthae*, both pseudosuchians from the Chañares Fm., display slow and moderate growth rates, respectively (Leucona et al., 2020; Ponce et al., 2024). In contrast, analyses of *Lagerpeton chanarensis*, a stem-avemetatarsalian, as well as *Lewisuchus admixtus*, a dinosuriform, both from the same horizon, suggest rapid growth (Garcia Marsà et al., 2017, 2020; Ezcurra et al., 2020). Other pseudosuchians, including the aetosaur *Aetosauroides scagliai* from the Ischigualasto Fm., exhibit moderate to slightly-fast growth (Ponce et al., 2022). Meanwhile, “rauisuchian” pseudosuchians such as *Saurosuchus galilei* and *Sillosuchus longicervix*, also from the Ischigualasto Fm., show clear rapid growth rates (Curry Rogers et al., 2024). Therefore, the acquirement of plasticity/flexibility in the growth and elevated growth rates were traits present already

in non-archosauriforms Archosauria and were continuous among several early Archosauria lineages during the Upper Triassic.

Intraskeletal variation

The increase in the studies focused in bone microstructure of proterochampsids in recent years allows to assess the variation of bone histology between different elements of the same individual. Thus, two well differentiated settings are observed. On the one hand, species such as *Gualosuchus reigi* and *Proterochampsa barrionuevoi* exhibit a conservative osteohistological configuration across all their sampled elements. Indeed, the humerus, femur and tibia of *G. reigi* PVL 4576 and the femur (Curry Rogers et al., 2024) and humerus of *P. barrionuevoi* PVSJ 606 show no significative differences in the bone matrix, vascularisation and CGM counting.

On the other hand, a strong diversity within the individuals of *Chanaresuchus bonapartei* is recognised. For example, intraskeletal variation was reported for the *C. bonapartei* PULR-V 116 specimen, since the tibia (fibrolamelar complex), femur (parallel-fibred bone) and fibula (lamellar bone) exhibit rapid, moderate to slow and slow growth rates, respectively (Garcia Marsà et al., 2023). In previous studies, other specimens of *C. bonapartei* have been examined, including the femur and an osteoderm from the specimens PVL 4575 (Ponce et al., 2021) and PVL 6244 (Cerda et al., 2015) respectively. In the current study, additional elements from these two specimens are incorporated into the sample: humerus and tibia of PVL 4575, and humerus, femur and a dorsal rib of PVL 6244. Then, the availability of a broad set of bones (appendicular, axial, and dermal) allows the assessment of intraskeletal variation in these two individuals.

Regarding the bone matrix of *C. bonapartei* PVL 6244 individual, both sampled appendicular bones (humerus and femur) show similar features: concentric layers of parallel-fibred and woven-fibred bone organised in a stratified arrangement. The

vascularisation also exhibits a stratified arrangement, reaching a laminar pattern in the femur, meanwhile in the humerus no particular vascular pattern is observed. The separation between these distinct layers of bone matrix and vascular density is marked by CGM (LAGs and/or annuli). The humerus displays up to three of these CGM and the femur records up to six (Fig. 8). Besides these differences in the number of CGM, the femur registers an additional fourth layer (located at the subperiosteal margin) with a clear increase in the bone deposition rate (higher degree of anisotropy and vascularisation) (Fig. 8). In this sense, the humerus and the femur are differentiated at vascular and CGM counting levels. Hence, the femur possessed a faster growth rate than the humerus. In respect to the dorsal rib, an even stronger heterogeneous histologic comparison is visible as well. In this sense, the rib had a faster growth rate in early stages of ontogeny, since this is composed of woven-fibred bone only. In addition, at least eight tightly grouped CGM are recorded in the subperiosteal margin (Fig. 8), which may imply differences for age estimation. Finally, the osteoderm of *C. bonapartei* PVL 6244, exhibit at least eight LAGs (Cerda et al., 2015), revealing a disparate variation regarding the number of CGM (Fig. 8).

In the case of *C. bonapartei* PVL 4575, the intraskeletal variation is minor in respect to PVL 6244 specimen. The femur and the humerus attained a slow to moderate growth rate based in the presence of parallel-fibred bone and isolated areas of woven-fibred bone (Ponce et al., 2021). Meanwhile, the tibia reached a slower growth rate since it is formed entirely by parallel-fibred bone. The vascularisation is rather constant in the three elements. Alternatively, the number of CGM is a variable parameter, recording one, none and three LAGs in the femur, tibia and humerus respectively. In comparison with *C. bonapartei* PULR-V 116, on which the same appendicular bones

were examined, greater differences on the bone matrix character are informed in the latter (Garcia Marsà et al., 2023).

The variation of the bones within the same individual is notable for *Chanaresuchus bonapartei*. The elements differ in counts of CGM, vascularization pattern and intrinsic fibres organisation of the bone matrix. Therefore, this variation indicates that different parts of *C. bonapartei* skeleton are capable of adopting distinct growth strategies. Explanation for this variation is likely linked to allometric growth, sexual dimorphism, biomechanical or physiological causes (Ricqlès et al., 1991; Reid, 1996; Curry, 1999; Starck and Chinsamy, 2002). Future studies should explore greatly the potential origin for this trait. Previous studies proposed a high intraspecific variation for Rhadinosuchinae clade based on their anatomical features (Ezcurra et al., 2016). This anatomical characterisation likely reflects deeper physiological differences among different taxa of Proterochampsidae. Finally, the marked intraskeletal variation indicates that reliable inferences about growth rates in this taxon are useful only when homologous skeletal elements from different individuals are considered.

Diverging lifestyles

The estimated lifestyles for most proterochampsids indicate a terrestrial habit (i.e., *Chanaresuchus bonapartei*, *Gualosuchus reigi*, *Pseudochampsa ischigualastenis* and *Tropidosuchus romeri*), except for *Proterochampsa barrionuevoi*, whose habit is ambiguous between aquatic and amphibious/terrestrial. Furthermore, although the binary statistical model (BSM) yields an amphibious/terrestrial lifestyle for the latter, its compactness profile is markedly different from the rest (Fig. 6). Previous studies that examined *P. barrionuevoi* PVSJ 606 reported non-fused neurocentral sutures but closed scapula-coracoids sutures in this specimen, precluding a robust inference regarding its ontogenetic stage (Trotteyn, 2011). However, the occurrence of the EFS supports, at least, the attainment of skeletal maturity. Likewise, the non-fused neurocentral sutures

582 in *P. barrionuevoi* seem to indicate an ecological adaptation instead, since this trait is
583 also present in choristoderans, ichthyosaurs and sauropterygians, forms with an aquatic
584 or amphibious habit (Heinrich et al., 2021). Thus, it is feasible to rule out a terrestrial
585 lifestyle for *P. barrionuevoi* and propose aquatic or amphibian habits for this taxon.
586 This inference is likely to be extended to *P. nodosa*, its Brazilian counterpart, because
587 of their anatomical similarities, such as broad dorsoventrally flattened skull and strongly
588 ornamented; external nares and orbits dorsally placed, semi-sprawling limb posture and
589 absence of osteoderms, among others (Simão-Oliveira, 2022).

590 The aquatic/amphibious habit of *Proterochampsa* contributed variation to the
591 lifestyles of the Proterochampsidae family. This difference is marked in the divergence
592 between the two subfamilies of the clade, with Proterochampsinae being aquatic or
593 amphibious and Rhadinosuchinae being terrestrial. Within a phylogenetic framework,
594 species with disparate habits at family level are also recorded in Doswelliidae, the sister
595 taxon of proterochampsids. For instance, *Vancleavea campi* has been interpreted as an
596 aquatic or amphibian taxon (Nesbitt et al., 2009), while other doswelliids such as
597 *Doswellia kaltenbachi* and *Jaxtasuchus salomoni* are considered to have an amphibious
598 or terrestrial lifestyle (Sues et al., 2013). In an even broader phylogenetic context,
599 considering non-Avialae Archosauria, in Phytosauria and Crocodylomorpha there are
600 recognised taxa with both aquatic and amphibian habits. Likewise, non-avian dinosaurs
601 such as *Spinosaurus* and *Baryonyx* are identified as possible amphibious taxa, in
602 comparison with other inferred terrestrial spinosaurids such as *Suchomimus*, based on
603 different analyses that include microanatomical studies (Fabbri et al., 2022). Then, the
604 presence of aquatic/amphibious lifestyles seems to have been acquired independently
605 several times in non-Avialae Archosauriformes.

606 ***Irregular quantitative growth rates***

607 Estimated growth rates obtained from femoral sections display a wide range. The
608 inferred annual and daily growth rates are greatly irregular, with some specimens
609 showing a decreasing rate towards the end of ontogeny (i.e., *Chanaresuchus bonapartei*
610 PVL 6244, Rhadinosuchinae indet. CRILAR-Pv 488 and *Tropidosuchus romeri* PVL
611 4606), whereas others appear to exhibit late stages of accelerated growth (i.e., *C.*
612 *bonapartei* PULR-V 125, *Pseudochampsa ischigualastensis* PVSJ 567 and *T. romeri*
613 PVL 4606). Specifically, *P. ischigualastensis* PVSJ 567 exhibits the maximum daily
614 perimeter and area are growth, but with only 4 fully traceable CGM (out of a total
615 potential of 13: 4 fully traceable+9 no traceable), an overestimation is clear for this. For
616 this reason, Rhadinosuchinae indet. CRILAR-PV 488 is considered a more suitable
617 proxy to approximate the maximum daily perimeter and area growth rate, since all their
618 observed CGM are continuous throughout the cortex. This exhibits values of 12 μm and
619 58 μm^2 (at fourth CGM stage) for these parameters, respectively. Conversely, *C.*
620 *bonapartei* PULR-V 125 reached the lowest values of daily growth rate, with 8 μm and
621 9 μm^2 (at first CGM stage) for the perimeter and the area, respectively. Likewise, *C.*
622 *bonapartei* PVL 6244, achieved higher growth rates, reflecting the developmentally
623 flexibility growth at quantitative approaches even. Finally, both samples of *T. romeri*
624 (PVL 4604 and 4606) attained similar values of daily perimeter (6–10 μm) and area
625 (11–16 μm^2) growth rates, although seem they achieved shorter lifespan (i.e., one year
626 old), likely indicative of juvenile stage.
627 These irregular growth rates resemble to those reported for extant crocodiles such as
628 *Caiman latirostris*, where the curve of the femoral growth rate, with some variations,
629 decreases through ontogeny (Pereyra et al., 2025). For this species, minimum and
630 maximum values of 0.12 mm and 5.73 mm as annual perimeter growth are informed,
631 respectively, while 0.66 mm^2 and 29.25 mm^2 are the respective minimum and maximum

values for annual area growth (Pereyra et al., 2025). However, this value of 29.25 mm^2 should be noted as for an outlier, and a range of 19–22 mm^2 is more confident for the evaluation of maximum annual area growth. In our sample, the minimum annual perimeter and area growth values (0.32 mm and 0.81 mm^2, respectively, in *Chanaresuchus bonapartei* PULR-V 125) are higher than those recorded for *C. latirostris*. Conversely, the maximum reliable values for annual perimeter and area growth (5.65 mm and 21.27 mm^2, respectively, in Rhadinosuchinae indet. CRILAR-Pv 488) are comparable to, or slightly higher than, those reported for *C. latirostris*. In this sense, proterochampsids appear to have achieved a faster initial femoral growth than *C. latirostris*, and subsequently, with clearly disparate variations, their growth slowed, but reached similar or upper rates during the later stages of ontogeny. However, in the absence of sampled hatchling and/or juvenile proterochampsids, these inferences should be treated with caution. Other comparable studies have been carried out in extant crocodylomorphs, but these are either based solely on juveniles of *Alligator mississippiensis* (Woodward et al., 2014) or use the humerus as a proxy element, as in *Araripesuchus* (Fernandez Dumont et al., 2021) and *Crocodylus niloticus* (Audije-Gil et al., 2023).

This quantitative method allows us to preliminary infer an irregular growth for proterochampsids, which apparently begins with a faster rate than extant crocodiles. Then, the growth continues with great variations, reaching slightly higher growth rates than crocodiles as ontogeny progresses. The diversity in the growth trajectories observed in *Chanaresuchus* and *Tropidosuchus* may indicate a strong condition of physiological susceptibility, expressed as developmentally flexibility growth in these species.

Conclusion

In summary, thus study reports proterochampsids with rapid (*Gualosuchus reigi*, although this is based for its juvenile stage), moderate to rapid (*Proterochampsa barrionuevoi*) and slow (*Pseudochampsa ischigualastensis*) growth rates. Other species, such as *Chanaresuchus bonapartei* and *Tropidosuchus romeri* displayed a wide range of growth strategies, suggesting a high physiological susceptibility, attaining an appreciable degree of developmentally flexibility growth, mainly in *C. bonapartei*. The latter also exhibits a strong component of intraskeletal variation, which implies that distinct sections of the skeleton had the ability to attain different growth rates. Statistical studies of the microanatomy, propose a clear division of the lifestyles within the group, with Proterochampsinae possessing aquatic of amphibious lifestyles and Rhadinosuchinae with terrestrial habits. Preliminary quantitative growth rate estimations suggest that proterochampsids exhibited growth rates similar to those of living crocodilians. Accordingly, both in the early and late stages of ontogeny, the values obtained were comparable to or only slightly higher than those recorded in the femur of *Caiman latirostris*. Future studies should integrate Brazilian forms and more complete ontogenetic series to reach strongly accurate interpretations.

Acknowledgments

We are thankful to the curators of the museums and institutes P. Ortiz (PVL, S.M. de Tucumán, Tucumán Argentina), R. Martínez and D. Abelín (PVSJ, San Juan City, San Juan, Argentina) for allowing us to observe and prepare the materials. In addition, we thank to I. Cerda (IIPG, General Roca, Río Negro, Argentina) for his advising and allowing us the use of ‘Laboratorio de Paleohistología’ (Museo Histórico y

Paleontológico Carlos Ameghino, Cipolletti, Río Negro, Argentina) to prepare the sections. Finally, we thank him, as well as Z. Kulik (AMNH, New York & FMNH, Chicago, U.S.A.) for their reviews. Funding: PICT 2018-00717 (ANPCyT) to JBD, Subsidio APA-Bunge & Born 2022 and Sepkosky Grant 2022 to DAP and PICT 2011-1652 to F.E. Novas.

References

Arcucci, A.B. (1990). Un nuevo Proterochampsidae (Reptilia– Archosauriformes) de la fauna local de Los Chañares (Triásico Medio), La Rioja, Argentina. *Ameghiniana*, *27*, 365–378.

Arcucci, A.B., Previtera, E., & Mancuso, A.C. (2019). Ecomorphology and bone microstructure of Proterochampsia from the Chañares Formation. *Acta Palaeontologica Polonica*, *64*, 157–170.

Audije-Gil, J., Barroso-Bercenilla, F., & Cambra-Moo, O. (2023). Mapping histovariability and growth patterns of *Crocodylus niloticus* bred in captivity and their paleobiological implications. In Woodward, H.L., & Farlow, W.O. (Eds.), *Ruling Reptiles, Crocodylian Biology and Archosaur Paleobiology* (pp. 284–299). Indiana University Press, Bloomington.

Barberena, M.C. (1982). Uma nova espécie de Proterocampsa (*Proterocampsa nodosa* sp. nov.) do Triássico do Brasil. *Anais Anais da Academia Brasileira de Ciencias*, *54*, 127–141.

Buffrénil, V. de, & Quilhac, A. (2021). Bone tissue types: a brief account of currently used categories. In Buffrénil, V. de, Ricqlès, A.J. de, Zylberberg, L., & Padian, K. (Eds.), *Vertebrate Skeletal Histology and Paleohistology* (pp. 147–182). CRC Press, Boca Raton & London.

709 Canoville, A., & Laurin, M. (2010). Evolution of humeral microanatomy and lifestyle in
710 amniotes, and some comments on palaeobiological inferences. *Biological Journal*
711 *of Linnean Society*, *100*, 384–406.
712 Canoville, A., & Laurin, M. (2009). Microanatomical diversity of the humerus and
713 lifestyle in lissamphibians. *Acta Zoologica*, *90*, 110–122.
714 Castanet, J., Francillon-Vieillot, H., Meunier, F.J., & Ricqlès, A. de (1993). Bone and
715 individual aging. In Hall, B.K. (Ed.), *Bone Growth* (pp. 245–283). CRC Press,
716 London.
717 Castanet, J., Rogers, K.C., Cubo, J., & Boisard, J.J. (2000). Periosteal bone growth rates
718 in extant ratites (ostriche and emu). Implications for assessing growth in
719 dinosaurs. *Comptes rendus de l'Academie des sciences. Serie III, Sciences de la*
720 *vie*, *323*, 543–550.
721 Cerda, I.A., Desojo, J.B., Trotteyn, M.J., & Scheyer, T.M. (2015). Osteoderm histology
722 of Proterochampsia and Doswelliidae (Reptilia: Archosauriformes) and their
723 evolutionary and paleobiological implications. *Journal of Morphology*, *276*, 385–
724 402.
725 Cerda I.A., Pereyra M.E., Garrone, M.C., Ponce D.A., Navarro, T.G., González R.,
726 Militello M., Luna, C., & Jannello, M.J. (2020). A basic guide for sampling and
727 preparation of extant and fossil bones for histological studies. *Publicación*
728 *Electrónica de Asociación Paleontológica Argentina*, *20*, 15–28.
729 Chinsamy, A. (2023). Palaeoecological deductions from osteohistology. *Biology*
730 *Letters*, *19*, 20230245.
731 Chinsamy-Turan, A. (2005). *The microstructure of dinosaur bone*. John Hopkins
732 University Press.

Colbert, E.H. (1960). A new Triassic Procolophonid from Pennsylvania. *American Museum Novitates*, *2022*, 1–19.

Cotuli-Cereda, A., Agnolín, F.L., Garcia Marsà, J.A., & Novas, F.E. (2026). New insights on the tarsus of *Chanaresuchus bonapartei* Romer, 1971 (Archosauriformes) and its evolutionary implications. *The Anatomical Record*, *309*, 2084–2099.

Curry, K.A. (1999). Ontogenetic histology of *Apatosaurus* (Dinosauria: Sauropoda) new insights on growth rates and longevity. *Journal of Vertebrate Paleontology*, 19, 654–665.

Curry Rogers, K., Martínez, R.N., Colombi, C., Rogers, R.R., & Alcober, O. (2024). Osteohistological insight into the growth dynamics of early dinosaurs and their contemporaries. *PLoS ONE*, *19*, e0298242.

Ezcurra, M.D. (2016). The phylogenetic relationships of basal archosauromorphs, with an emphasis on the systematics of proterosuchian archosauriforms. *PeerJ*, *4*, e1778.

Ezcurra, M.D., & Sues, H.-D. (2021). A re-assessment of the osteology and phylogenetic relationships of the enigmatic, large-headed reptile *Sphodrosaurus pennsylvanicus* (Late Triassic, Pennsylvania, USA) indicates archosauriform affinities. *Journal of Systematic Palaeontology*, *19*, 1643–1677.

Ezcurra, M.D., Lecuona, A., & Martinelli, A. (2010). A new basal archosauriform diapsid from the Lower Triassic of Argentina. *Journal of Vertebrate Paleontology*, *30*, 1433–1450.

Ezcurra, M.D., Montefeltro, F.C., Pinheiro, F.L., Trotteyn, M.J., Gentil, A.R., Lehmann, O.E.R., & Pradelli, L.A. (2021). The stem-archosaur evolutionary radiation in South America. *Journal of South American Earth Sciences*, *110*, 102935.

Fabbri, M., Navalón, G., Benson, R.B.J., Pol, D., O'Connor, J., Bhullar, B.S., Erickson, G.M., Norell, M.A., Orkney, A., Lamanna, M.C., Zouhri, S., Becker, J., Emke, A., Dal Sasso, C., Bindellini, G., Maganuco, S., Auditore, M., & Ibrahim, N. (2022). Subaqueous foraging among carnivorous dinosaurs. *Nature*, *7903*, 852–857.

Fernandez Dumont, M.L., Pereyra, M.E., Bona, P., & Apesteguía, S. (2021). New data on the palaeosteohistology and growth dynamic of the notosuchian *Araripesuchus* Price, 1959. *Lethaia*, *54*, 578–590.

Francillon-Vieillot, H., Buffrénil, V. de, Castanet. J., Géraudie. J., Meunier, F.J., Sire, J.-Y., Zylberberg, L., & Ricqlès, A. de (1990). In Carter, J. (Ed.), *Skeletal Biomineralizations: Patterns, Processes and Evolutionary Trends Vol. 1: Microstructures and mineralization of vertebrate skeletal tissues* (pp. 471–530). Van Nostrand Reinhold, New York.

Garcia Marsà, J.A., Agnolín, F.L., & Novas, F.E. (2020). Comparative bone microstructure of three archosauromorphs from the Carnian, Late Triassic Chañares Formation of Argentina. *Acta Palaeontologca Polonica*, *65*, 387–398.

Garcia Marsà J.A., Ponce, D.A., Agnolín, F.L., & Novas, F.E. (2023). Histovariability and lifestyle in Proterochampsidae Romer, 1966 (Archosauriformes) from the Chañares Formation (Late Triassic), northwestern Argentina. *Comptes Rendus Palevol*, *22*, 606–622.

Germain, D., & Laurin, M. (2005). Microanatomy of the radius and lifestyle in amniotes (Vertebrata, Tetrapoda). *Zoologica Scripta*, *34*, 335–350.

Girondot, M., & Laurin, M. (2003). Bone profiler: a tool to quantify, model, and statistically compare bone-section compactness profiles. *Journal of Vertebrate Paleontology*, *23*, 458–461.

Gônet, J., Michel, L., & Girondot, M. (2022). BoneProfileR: The next step to quantify, model, and statistically compare bone section compactness profiles. *Palaeontologia Electronica*, 25.a12. https://doi.org/10.26879/1194

Heinrich, C., Paes Neto, V.D., Lacerda, M.B., Martinelli, A.G., Fiedler, M.S., & Schultz, C.L. (2021). The ontogenetic pattern of neurocentral suture closure in the axial skeleton of Hyperodapedontinae (Archosauromorpha, Rhynchosauria) and its evolutionary implications. Palaeontology, *64*, 409–427.

Huene, F. von. (1938). Die fossilen Reptilien des südamerikanischen Gondwanalandes. *Neues Jahrbuch Mineralogie, Geologie und Paläontologie*, *1938*, 142–151.

Kriloff, A., Germain, D., Canoville, A., Vincent, P., Sache, M., & Laurin, M. (2008). Evolution of bone microanatomy of the tetrapod tibia and its use in palaeobiological inference. *Journal of Evolutionary Biology*, *21*, 807–826.

Laurin, M., & Buffrénil, V. de (2015). Microstructural features of the femur in early ophiacodontids: A reappraisal of ancestral habitat use and lifestyle of amniotes. *Comptes Rendus Palevol*, *15*, 115–127.

Laurin, M., Girondot, M., & Loth, M.M. (2004). The evolution of long bone microanatomy and lifestyle in lissamphibians. *Paleobiology*, *30*, 589–613.

Lecuona, A., Desojo, J.B. & Cerda, I.A. (2020). New information on the anatomy and histology of *Gracilisuchus stipanicicorum* (Archosauria: Pseudosuchia) from the Chañares Formation (early Carnian), Argentina. *Comptes Rendus Palevol*, *19*, 40–62.

Mamani, C.A. (2026). *Anatomía, filogenia y paleobiología de* Tropidosuchus *Arcucci 1990 (Archosauriformes: Proterochampsidae)* [Ph.D. thesis, Universidad de Buenos Aires].

Müller. R.T. (2025). New proterochampsid remains from the Middle Triassic of Brazil enhance the group's diversity during its origins. *The Science of Nature*, *112*, 28.

Nesbitt, S.J., Stocker, M.R., Small, B.J. & Downs, A. (2009). The osteology and relationships of *Vancleavea campi* (Reptilia: Archosauriformes). *Zoological Journal of the Linnean Society*, *157*, 814–864.

Padian, K., & Stein, K. (2013). Evolution of growth rates and their implications. In Padian, K., & Lamm, E.T. (Eds.), *Bone Histology of Fossil Tetrapods* (pp. 253–264). California University Press, Berkeley.

Paes-Neto, V.D., Lacerda, M B., Ezcurra, M.D., Raugust, T., Trotteyn, M.J., Soares, M.B., Schultz, C.L., Pretto, F.A., Francischini, H., & Martinelli, A.G. (2024). New rhadinosuchine proterochampsids from the late Middle-early Late Triassic of southern Brazil enhance the diversity of archosauriforms. *The Anatomical Record*, *307*, 851–889.

Pereyra, M.E, Bona, P., Siroski, P., & Chinsamy, A. (2025). Analyzing the life history of caimans: the growth dynamics of *Caiman latirostris* from an osteohistological approach. *Journal of Morphology*, *286*, e70010.

Ponce, D.A., Cerda I.A., Desojo, J.B., & Nesbitt, S.J. (2017). The osteoderm microstructure of *Doswellia kaltenbachi*, *Vancleavea campi*, and *Chanaresuchus bonapartei* and its implications for palaeobiology of stem archosaurs. *Acta Palaeontologica Polonica*, *62*, 819–831.

Ponce, D.A., Cerda, I.A., & Desojo, J.B. (2024). First record of palaeopathologies in appendicular bones of the Triassic pseudosuchians Erpetosuchidae and Aetosauria based on microstructural approaches. *Acta Palaeontologica Polonica*, *69*, 395–402.

Ponce, D.A., Desojo, J.B., & Cerda, I.A. (2022). Palaeobiological inferences of the aetosaur *Aetosauroides scagliai* (Archosauria: Pseudosuchia) based on microstructural analyses of its appendicular bones. *Historical Biology*, *35*, 303–314.

Ponce, D.A., Trotteyn M.J., Cerda I.A., Fiorelli, L.E., & Desojo, J.B. (2021). Osteohistology and paleobiological inferences of proterochampsids (Eucrocopoda: Proterochampsia) from the Chañares Formation (late Ladinian–early Carnian), La Rioja, Argentina. *Journal of Vertebrate Paleontology*, *41*, e1926273.

Price, L.I. (1946). Sobre um novo pseudosúquio do Triássico Superior do Rio Grande do Sul. *Boletim Divisão de Geologia e Mineralogia*, *120*, 1–38.

Quémeneur, S., Buffrénil. V. de, & Laurin, M. (2013). Microanatomy of the amniote femur & inference of lifestyle in limbed vertebrates. *Biological Journal of Linnean Society*, *109*, 644–655.

Reid, R.E.H. (1996). Bone histology of the Cleveland-Lloyd dinosaurs and of dinosaurs in general, Part I. Introduction: introduction to bone tissues. *Brigham Young University Geology Studies*, 41, 25–72.

Reig, O.A. (1959). Primeros datos descriptivos sobre nuevos reptiles arcosaurios del Triásico de Ischigualasto (San Juan, Argentina). *Revista de la Asociación Geológica Argentina*, *13*, 257–270.

Ricqles, A. de; Meunier. F.J.; Castanet, J., & Francillon-Vieillot, E. (1991). Comparative microstructure of bone. In Hall, B.K. (Ed.), *Bone, Bone Matrix and Bone Specific Products. Vol. 3* (pp. 1–75). CRC Press, Boca Raton.

Romer, A.S. (1971). The Chañares (Argentina) Triassic reptile fauna. XI. Two new long-snouted thecodonts, *Chanaresuchus* and *Gualosuchus*. *Breviora*, *379*, 1–22.

Sander, P.M., Klein, N., Buffetaut, E., Cuny, G., Suteethorn, V., & Le Loeuff, J. (2004). Adaptive radiation in sauropod dinosaurs: bone histology indicates rapid evolution of giant body size through acceleration. *Organisms Diversity & Evolution*, *4*, 165–173.

Schneider, C., Rasband, W., & Eliceiri, K. (2012). NIH Image to ImageJ: 25 years of image analysis. *Nature Methods*, *9*, 671–675.

Starck, J.M., & Chinsamy, A. (2002). Bone microstructure and developmental plasticity in birds and other dinosaurs. *Journal of Morphology*, 254, 232–246.

Simão-Oliveira, D., de, Pinheiro, F.L., Andrade, M.B. de, & Pretto, F.A. (2022). Redescription, taxonomic revaluation and phylogenetic affinities of *Proterochampsa nodosa* (Archosauriformes: Proterochampsidae) from the early Late Triassic of the Candelaria Sequence (Santa Maria Supersequence). *Zoological Journal of the Linnean Society*, *196*, 1310–1332.

Simão-Oliveira, D., de, Santos, T. dos, Pinheiro, F.L., & Pretto, F.A. (2024). Assessing the adductor musculature and jaw mechanics of *Proterochampsa nodosa* (Archosauriformes: Proterochampsidae) through finite element analysis. *The Anatomica Record*, *307*, 1300–1314.

Sues, H.-D., Desojo, J.B., & Ezcurra, M.D. (2013). Doswelliidae: A clade of unusual armoured archosauriforms from the Middle and Late Triassic. In Nesbitt, S.J., Desojo J.B., & Irmis, R.B. (Eds.), *Anatomy, Phylogeny and Palaeobiology of Early Archosaurs and their Kin* (pp. 49–58). Geological Society of London Special Publication 379, London.

Trotteyn, M.J. (2011). Material Postcraneano de *Proterochampsa barrionuevoi* Reig 1959 (Diapsida: Archosauriformes) del Triásico Superior del Centro-oeste de Argentina. *Ameghiniana*, *48*, 424–446.

Trotteyn, M.J., Arcucci, A.B., & Raugust, T. (2013). Proterochampsia: an endemic archosauriform clade from South America. In Nesbitt, S.J., Desojo J.B., & Irmis, R.B. (Eds.), *Anatomy, Phylogeny and Palaeobiology of Early Archosaurs and their Kin* (pp. 59–90). Geological Society of London Special Publication 379, London.

Trotteyn, M.J., & Ezcurra, M.D. (2014). Osteology of *Pseudochampsa ischigualastensis* gen. et comb. nov. (Archosauriformes: Proterochampsidae) from the early Late Triassic Ischigualasto Formation of northwestern Argentina. *PloS ONE*, *9*, e111388.

Trotteyn, M.J., & Paulina-Carabajal, A. (2016). Braincase and neuroanatomy of *Pseudochampsa ischigualastensis* and *Tropidosuchus romeri* (Archosauriformes, Proterochampsia). *Ameghiniana*, *53*, 527–542.

Woodward, H.L., Horner, J.R. & Farlow, J.O. (2014). Quantification of intraskeletal histovariability in *Alligator mississippiensis* and implications for vertebrate osteohistology. *PeerJ*, *2*, e422.

Wu, Y., Malinverno, A., Meyers, S.R. & Hinnov, L.A. (2024). A 650-Myr history of Earth's axial precession frequency and the evolution of the Earth-Moon system derived from cyclostratigraphy. *Science advances*, *10*, eado2412.

Figure captions

Figure 1. Sampled bone elements of Argentinean proterochampsids in the current study. **A,** Humerus of the holotype of *Proterochampsa barrionuevoi* PVSJ 606; **B,** Femur of *Tropidosuchus romeri* PVL 4602; **C–E,** Humerus (C), femur (D) and tibia (E) of *Gualosuchus reigi* PVL 4576; **F, G,** Humerus (F) and tibia (G) of *Chanaresuchus bonapartei* PVL 4575; **H, I**, Humerus (H) and femur (I) of *C. bonapartei* PVL 6244. We do not count with images of the dorsal rib of *C. bonapartei* PVL 6244 prior sectioning. Abbreviations: DIS, distal.

(planned for one column width)

Figure 2. Bone histology of *Proterochampsa barrionuevoi* PVSJ 606. The inset boxes indicate the position of the detailed images in the figure. **A,** Complete humeral transverse section; **B,** View of the cortex, showing its woven-fibred bone (WFB) nature and some radial canals; **C**, Larger view of the cortex with some secondary osteons (OS) and WFB. **D–F**, Detail of the bone matrix and radial vascularisation; **G,** Detailed view of the external fundamental system (EFS); A, D, G: plane polarised light; B, C, F: cross polarised light (λ); E: cross-polarised light.

(planned for one column width)

Figure 3. Bone histology of *Tropidosuchus romeri* PVL 4602. The inset boxes indicate the position of the detailed images in the figure. **A, B,** Complete femoral transverse sections; **C,** Detail of the cortex, composed by woven-fibred bone (WFB) and moderate vascularisation acquiring a laminar or reticular pattern in some areas. A: plane polarised light; C: cross-polarised light (λ); D: cross polarised light (λ).

(planned for half-page width)

Figure 4. Bone histology of *Gualosuchus reigi* PVL 4576. The inset boxes indicate the position of the detailed images in the figure. **A, B, C**; Complete humeral (A), femoral (B) and tibial (C) complete transverse sections of *G. reigi* PVL 4576; **C–E,** View of the cortices, whose show a fibrolamellar complex (FLC) composition alongside an abundant vascularisation with a reticular orientation in some particular areas. A–C: plane polarised light; D–F: plane polarised light+cross polarised light (λ).

(planned for full-page width)

Figure 5. Bone histology of *Chanaresuchus bonapartei* PVL 4575 and *C. bonapartei* PVL 6244. The inset boxes indicate the position of the detailed images in the figure. **A, B,** Complete humeral (A) and tibial (B) transverse sections of *C. bonapartei* PVL 4575. **C,** View of the humeral cortex, formed by parallel-fibred bone (PFB) and a strong vascularisation in reticular pattern; **D,** View of other portion of the humeral cortex, composed by a presumably woven-fibred tissue (WFB) and dominated by radial canals; **E,** Detail of the femoral cortex, highly vascularised in a laminar pattern on a PFB matrix; **F–H**, Complete humeral (F), femoral (G) and that of dorsal rib (H) transverse sections of *C. bonapartei* PVL 6244; **I**, Detail on the humeral cortex, stratified in layers of WFB and PFB (i.e., zonal bone) with a rather scarce vascularisation; **J,** Close up of the femoral cortex. Unlike the humerus, the alternating structure of layers of WFB and PFB are clearer and the vascularisation reaches a laminar orientation in some areas; **K,** Dorsal rib histology. Detail of the cortex and part of the medullary region showing intertrabecular spaces (its). The perimedullary and the outer cortex are formed by poorly vascularised WFB and lamellar bone (LB) respectively, besides an external fundamental

system (EFS) is observed. Green-solid lines point CGM and the arrowheads indicate the continuity of them. A, B, F–H: plane polarised light; C–E, I–K: plane polarised light+cross polarised light (λ).

(planned for full-page width)

Figure 6. Binarized images, observed compactness (OC) and profile compactness, obtained by Bone ProfileR for selected Proterochampsidae elements. **A, B,** Humerus (A) and femur (B) of *Proterochampsa barrionuevoi* PVSJ 606; **C,** Femur of *Tropidosuchus romeri* PVL 4602; **D, E,** Humerus (D) and femur (E) of *Gualosuchus reigi* PVL 4576; **F,** Femur of *Pseudochampsa ischigualastensis* PVSJ 567. Red dotted curve represents the trajectory of compactness through the section, while blue solid curve represents the results of the global values of the profile.

(planned for full-page width)

Figure 7. Lines with markers graphs showing the quantitative growth trajectory attained by the sampled Argentinean proterochampsids. **Abbreviations**: **CGM**, cyclical growth mark; **MC**, medullary cavity; **SPS**, subperiosteal surface.

(planned for full-page width)

Figure 8. Skeletal reconstruction of *Chanaresuchus bonapartei* (modified from Trotteyn et al., 2013). Schemes of the different types of histological arrangement (i.e., intraskeletal variation) reached by the PVL 6244 specimen are added, based on appendicular, axial and dermal bones (Cerda et al., 2015). **Abbreviations**: **LAGs**, lines of arrested growth.

(planned for full-page width)

975 **Tables**

976

Table 1. Novel proterochampsid specimens histologically examined in the current study.

Taxon	Collection code	Element/s	BL	Locality	Horizon and age
Proterochampsinae					
Proterochampsa barrionuevoi	PVSJ 606[H]	Humerus	111 mm	Cancha de Bochas, Ischigualasto Prov. Park, San Juan, Argentina	Fm. Ischigualasto (Upper Triassic, late Carnian–early Norian)
Rhadinosuchinae					
Tropidosuchus romeri	PVL 4602	Femur	55 mm	Talampaya Nat. Park, La Rioja, Argentina	Chañares Fm. (Upper Triassic, early–middle Carnian)
Gualosuchus reigi	PVL 4576	Humerus	60 mm	Talampaya Nat. Park, La Rioja, Argentina	Chañares Fm. (Upper Triassic, early–middle Carnian)
		Femur	91 mm		
		Tibia	64 mm		
Chanaresuchus bonapartei	PVL 4575	Humerus	69 mm	Talampaya Nat. Park, La Rioja, Argentina	Chañares Fm. (Upper Triassic, early–middle Carnian)
		Tibia	83 mm		
Chanaresuchus bonapartei	PVL 6244	Humerus	98 mm	Talampaya Nat. Park, La Rioja, Argentina	Chañares Fm. (Upper Triassic, early–middle Carnian)
		Femur	151 mm		
		Dorsal rib	N/A		

Abbreviations: **BL**, bone length; **H**, holotype; **N/A**, no available information.

977

978

979

Table 2. Summary of the main osteohistological data of *Chanaresuchus bonapartei* and *Tropidosuchus romeri* femora reported to date.

Specimen	BL	Bone matrix	Vascularisation	CGM & tissue structures	Reference
Chanaresuchus bonapartei					
PULR-V 116	71 mm	PFB	Poor, with PO mainly	1 LAGs	Garcia Marsà et al., 2023
PULR-V 125	73 mm	ZB, alternated layers of PFB	High, reticular in some areas	3 annuli, EFS?	Garcia Marsà et al., 2020
PVL 4575	112 mm	Mainly PFB with patches of WFB	High, in a reticular pattern	1 LAG^{NT}, ICL	Ponce et al., 2021
PVL 6244	151 mm	ZB, alternated layers of PFB and WFB	Stratified in layers of low/high density	6 annuli$^{(4\ NT)}$	This study
Tropidosuchus romeri					
PVL 4606	48 mm*	PFB	High, laminar pattern in some areas	3 LAGs$^{(2\ NT)}$, ICL	Garcia Marsà et al., 2023
PVL 4602	55 mm	WFB	Moderate, often in a reticular pattern	No recorded	This study
PVL 4604	65 mm	FLC and PFB toward subperiosteum	High, PO and LC	1 LAGs, ICL	Garcia Marsà et al., 2020

Abbreviations and notes: *****fragmentary element; **BL**, bone length; **CGM**, cyclical growth marks; **EFS**, external fundamental system; **FLC**, fibrolamellar complex; **ICL**, internal circumferential layer; **LC**, longitudinal canals; **NT**, no traceable CGM; **PFB**, parallel-fibred bone; **PO**, primary osteons; **WFB**, woven-fibred bone; **ZB**, zonal bone.

980

981 **Supplementary Online Information**. 2 figures, 2 tables.

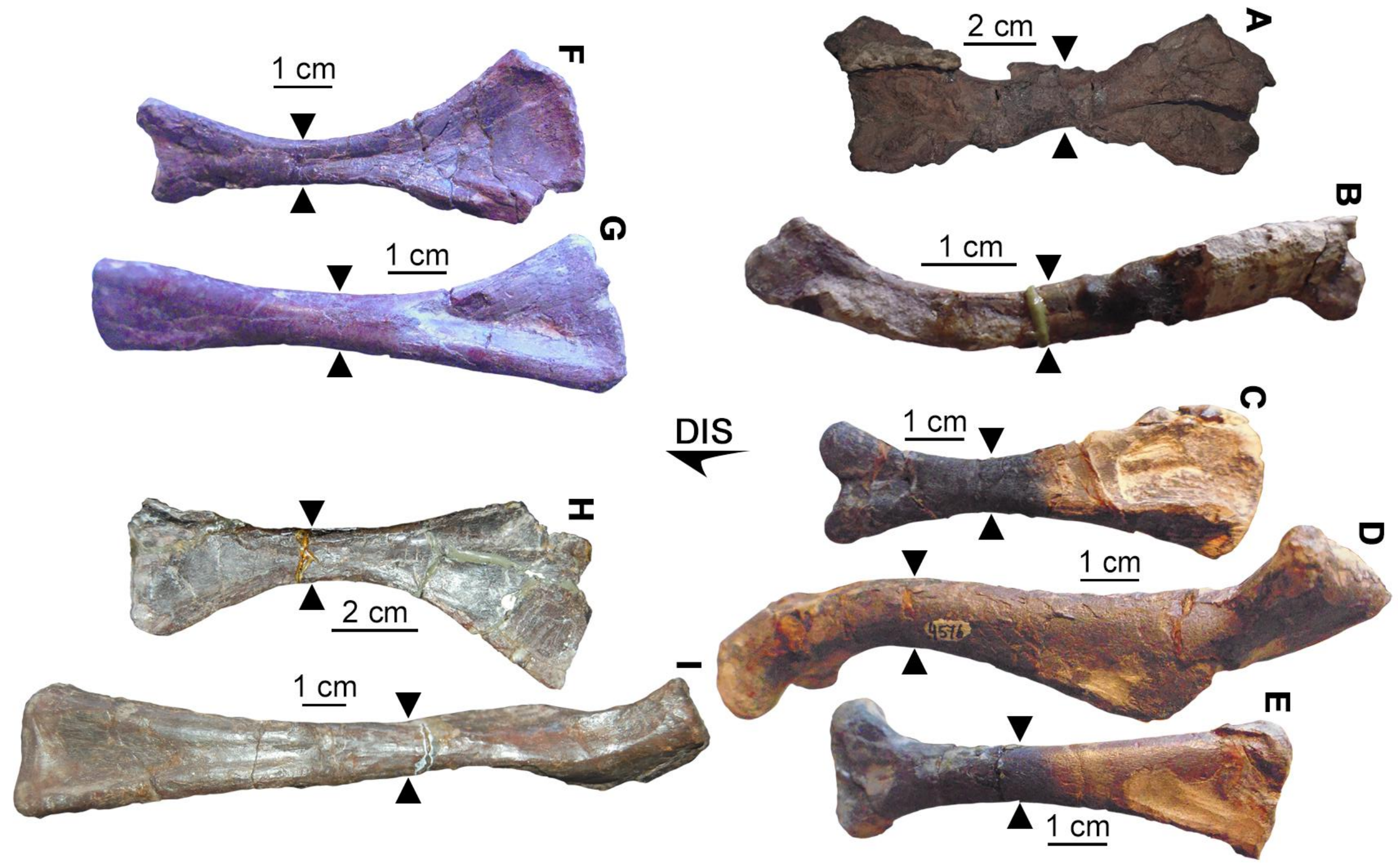
A
2 cm
B
1 cm
C
1 cm
DIS
D
1 cm
4576
E
1 cm
F
1 cm
G
1 cm
H
2 cm
I
1 cm

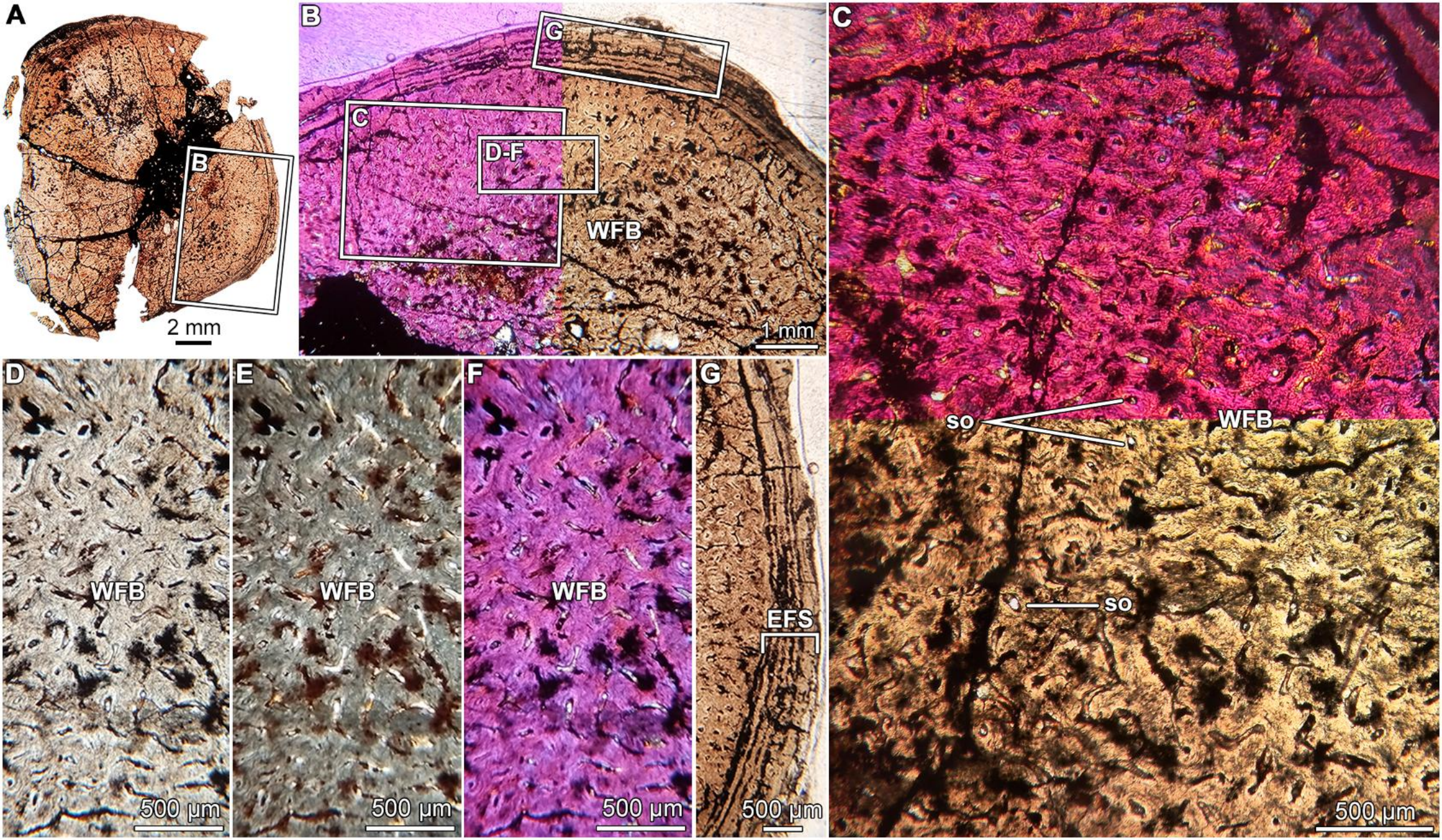
A
B
2 mm
B
G
C
D-F
WFB
1 mm
C
SO
WFB
SO
500 µm
D
WFB
500 µm
E
WFB
500 µm
F
WFB
500 µm
G
EFS
500 µm

A

C

D

1 mm

B

C

D

C

WFB

300 µm

D

WFB

500 µm

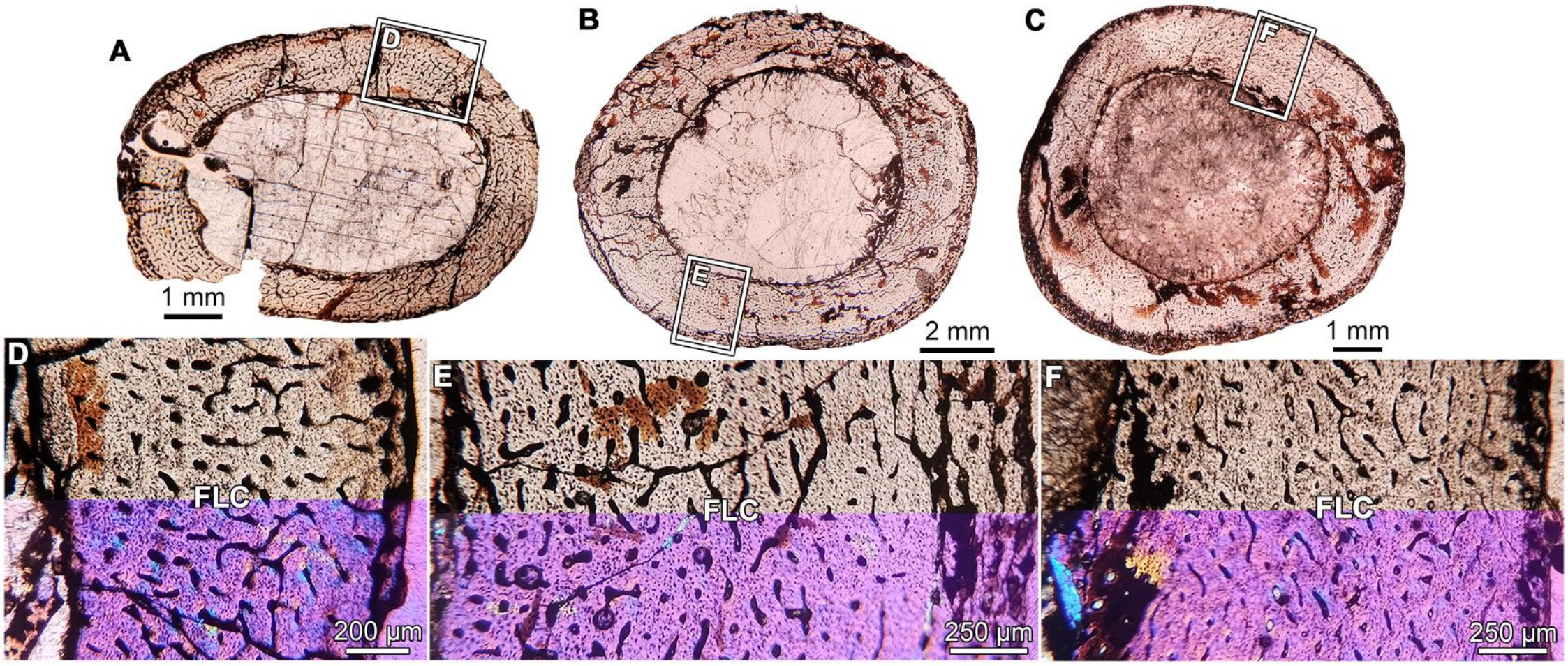
A
D
1 mm
B
E
2 mm
C
F
1 mm
D
FLC
200 µm
E
FLC
250 µm
F
FLC
250 µm

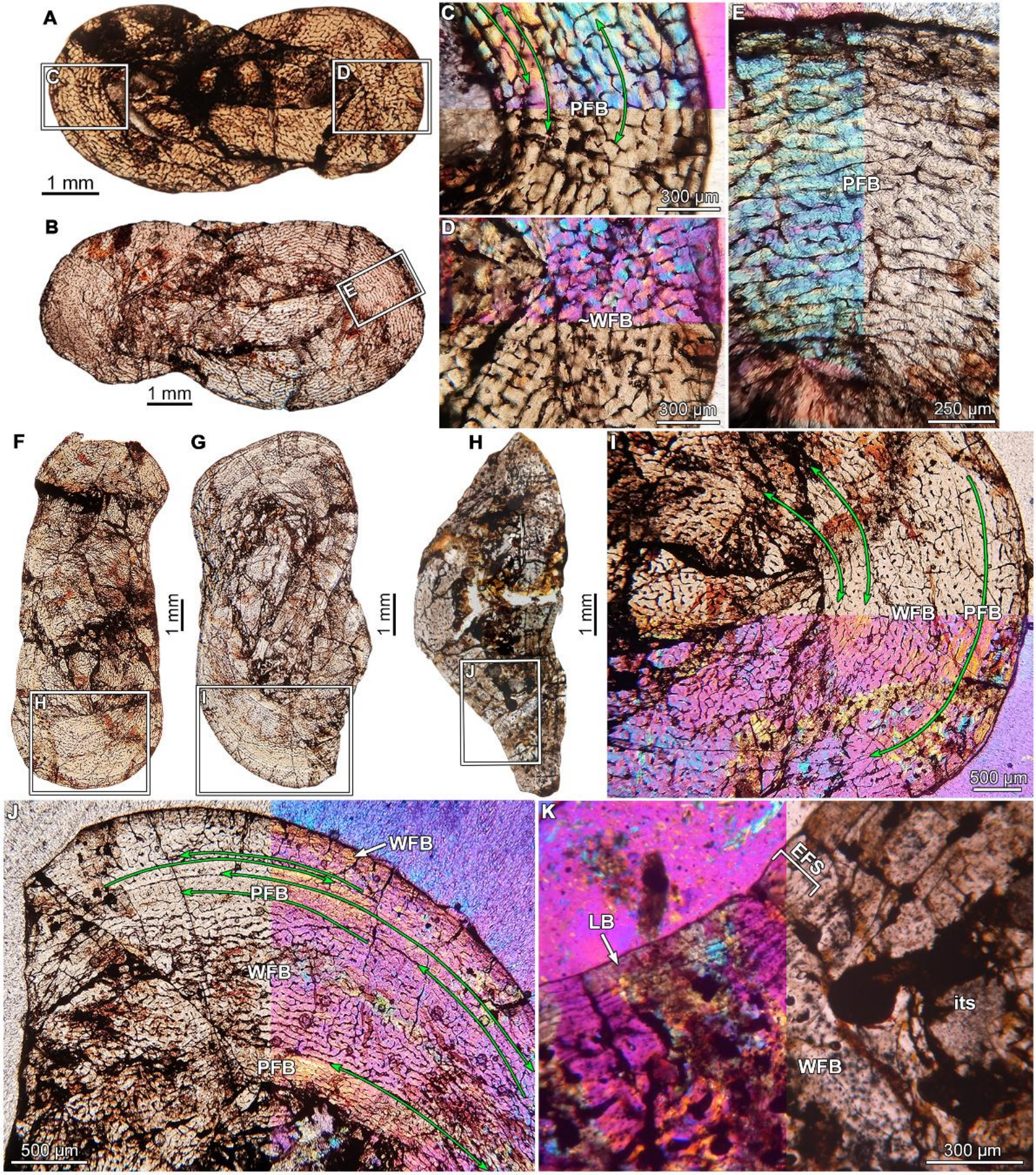
A
C
D
1 mm
B
E
1 mm
C
PFB
300 µm
D
~WFB
300 µm
E
PFB
250 µm
F
H
1 mm
G
I
1 mm
H
J
1 mm
I
WFB
PFB
500 µm
J
WFB
PFB
WFB
PFB
500 µm
K
LB
EFS
its
WFB
300 µm

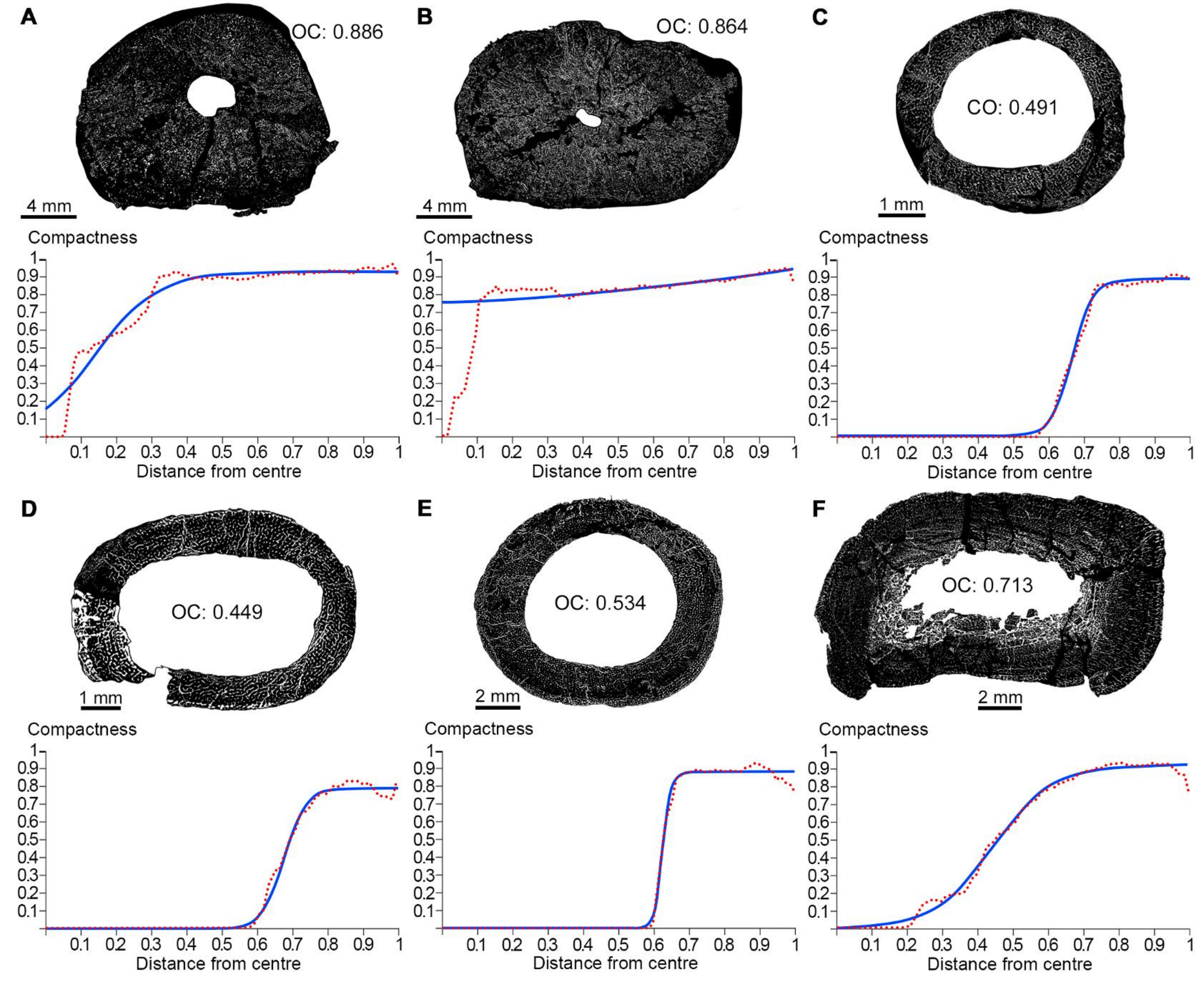
A
OC: 0.886
4 mm
B
OC: 0.864
4 mm
C
CO: 0.491
1 mm
Compactness
Distance from centre
D
OC: 0.449
1 mm
E
OC: 0.534
2 mm
F
OC: 0.713
2 mm

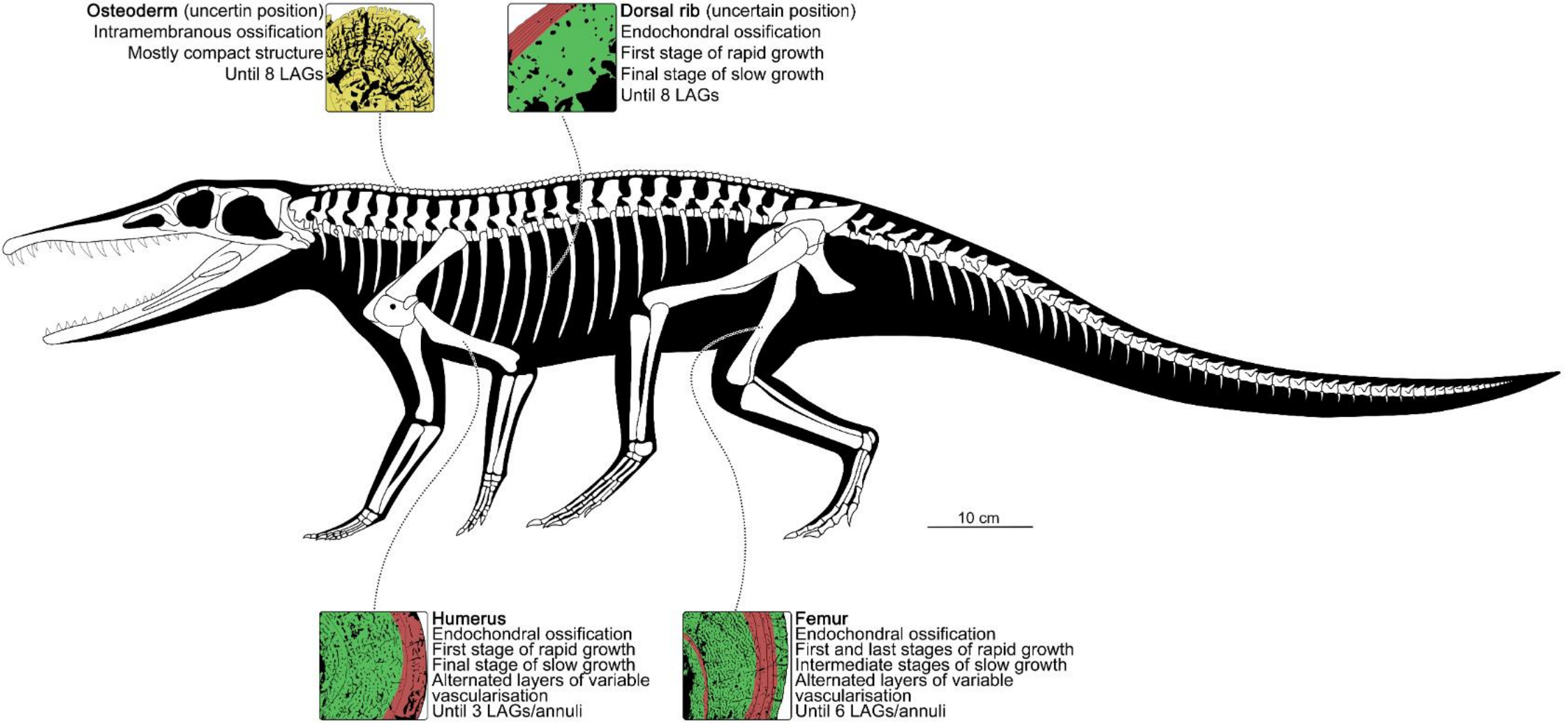
Osteoderm (uncertin position)
Intramembranous ossification
Mostly compact structure
Until 8 LAGs
Dorsal rib (uncertain position)
Endochondral ossification
First stage of rapid growth
Final stage of slow growth
Until 8 LAGs
10 cm
Humerus
Endochondral ossification
First stage of rapid growth
Final stage of slow growth
Alternated layers of variable vascularisation
Until 3 LAGs/annuli
Femur
Endochondral ossification
First and last stages of rapid growth
Intermediate stages of slow growth
Alternated layers of variable vascularisation
Until 6 LAGs/annuli

Perimmeter cumulative growth

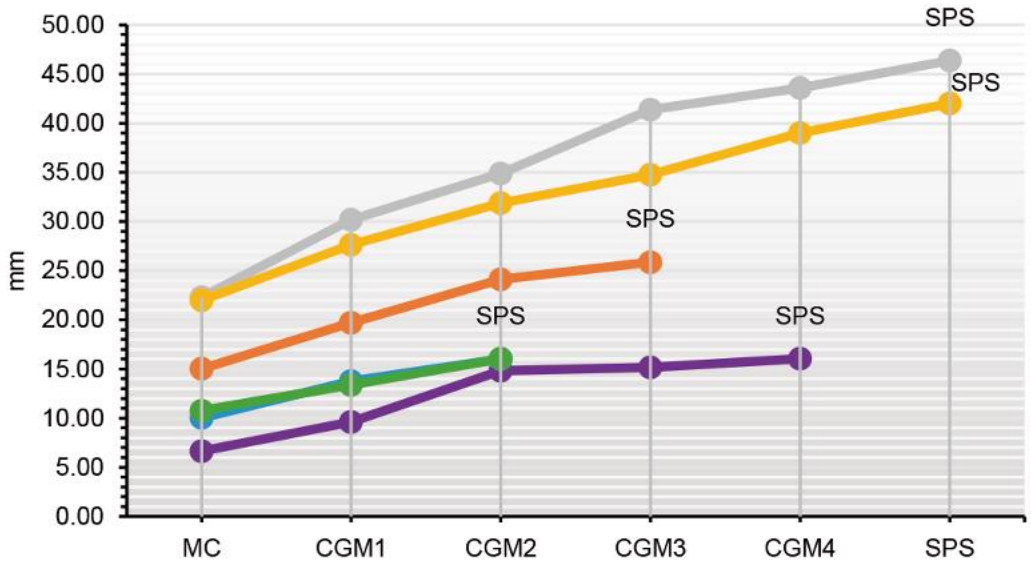

Area cumulative growth

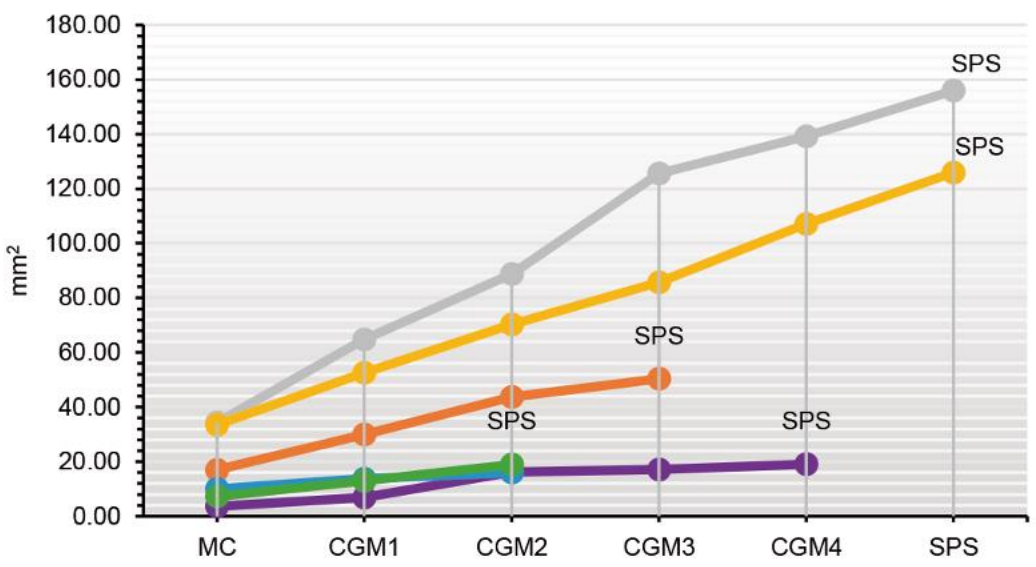

Annual perimeter growth

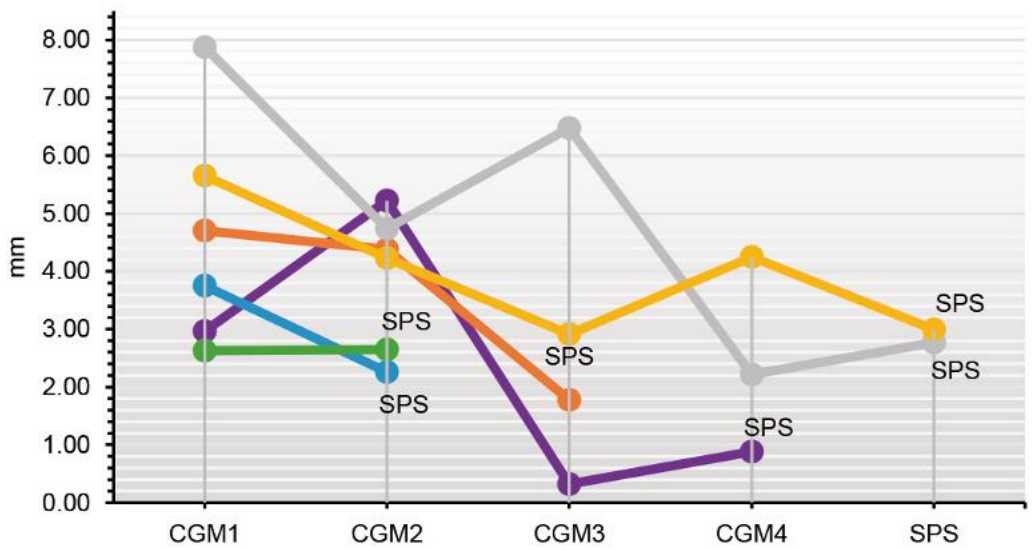

Annual area growth

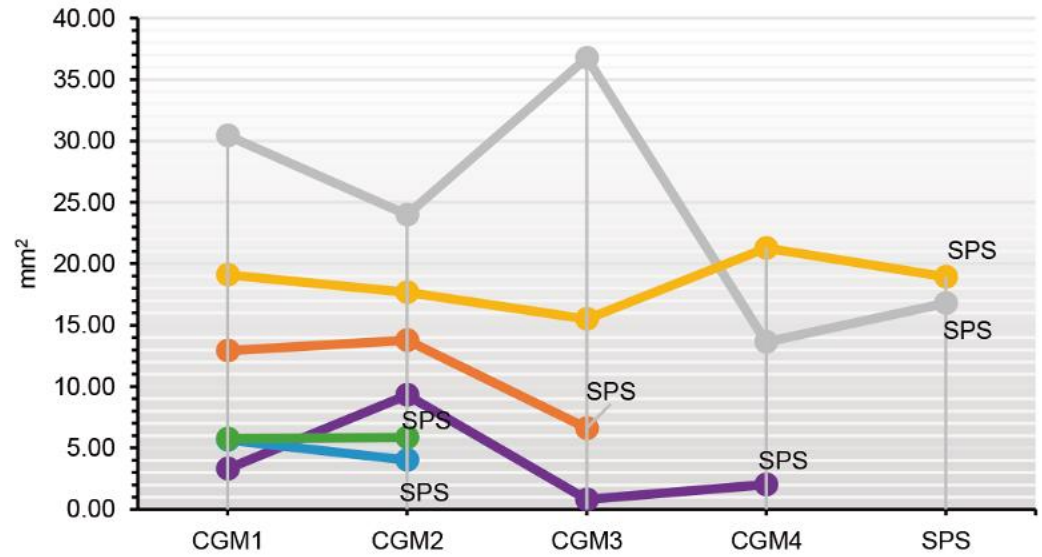

Daily perimeter growth

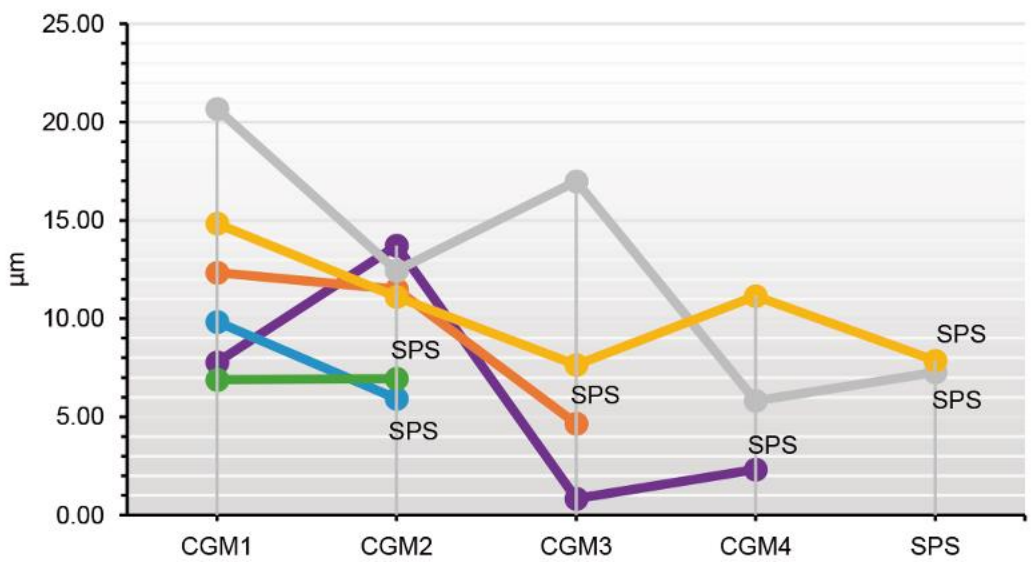

Daily area growth

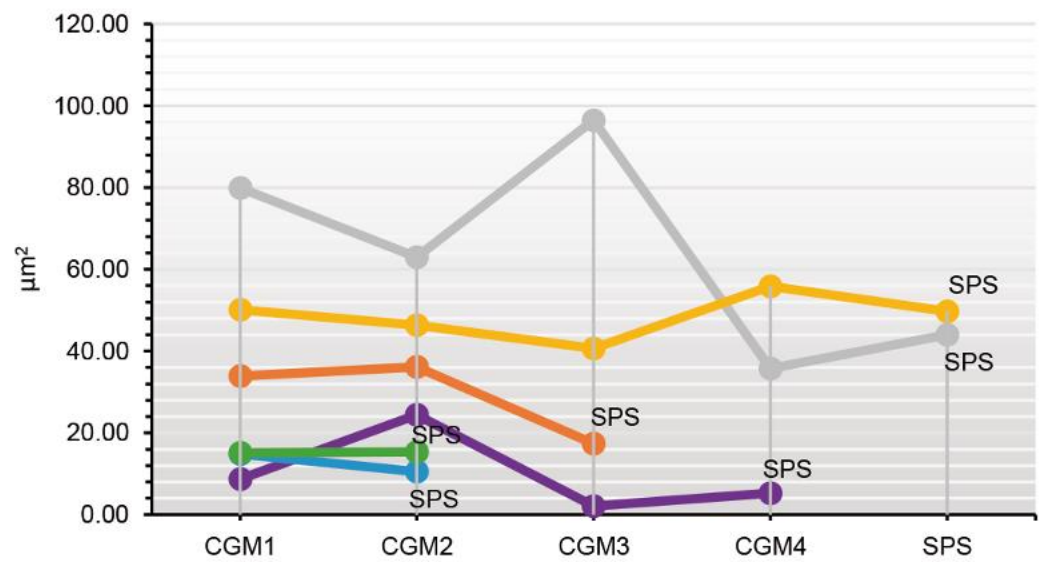

Chanaresuchus bonapartei PULR-V 125
Chanaresuchus bonapartei PVL 6244
Pseudochampsa ischigualastensis PVSJ 567
Rhadinosuchinae indet. CRILAR-Pv 488
Tropidosuchus romeri PVL 4604
Tropidosuchus romeri PVL 4606